3-10-2022

Direct Radiative Effect (DRE) of Dust Aerosols on West African and East Asian Monsoon: The Role of Ocean-Atmosphere Interactions

Anqi Wang

Xiaoning Xie

Xiaodong Liu

Zhi-Yong Yin

JGR Atmospheres

RESEARCH ARTICLE
10.1029/2021JD035917

Direct Radiative Effect (DRE) of Dust Aerosols on West African and East Asian Monsoon: The Role of Ocean-Atmosphere Interactions

Anqi Wang[1,2], Xiaoning Xie[1,3], Xiaodong Liu[1,2], and Zhi-Yong Yin[4]

[1]State Key Laboratory of Loess and Quaternary Geology, Institute of Earth Environment, Chinese Academy of Sciences, Xi'an, China, [2]University of Chinese Academy of Sciences, Beijing, China, [3]CAS Center for Excellence in Quaternary Science and Global Change, Xi'an, China, [4]Department of Environmental & Ocean Sciences, University of San Diego, San Diego, CA, USA

Key Points:

- Dust direct radiative effect (DRE) induces a surface cooling of the downstream ocean of the dust source region
- Dust DRE significantly causes the West African summer monsoon (WASM) strengthening and East Asian summer monsoon (EASM) weakening through ocean-atmosphere interactions
- Distinct DREs on WASM and EASM are dependent on relative locations of the ocean cooling regions to the respective monsoon regions

Supporting Information:

Supporting Information may be found in the online version of this article.

Correspondence to:

X. Xie,
xnxie@ieecas.cn

Citation:

Wang, A., Xie, X., Liu, X., & Yin, Z.-Y. (2022). Direct radiative effect (DRE) of dust aerosols on West African and East Asian monsoon: The role of ocean-atmosphere interactions. *Journal of Geophysical Research: Atmospheres*, *127*, e2021JD035917. https://doi.org/10.1029/2021JD035917

Received 23 SEP 2021
Accepted 3 MAR 2022

Author Contributions:

Conceptualization: Anqi Wang, Xiaodong Liu
Data curation: Anqi Wang
Formal analysis: Anqi Wang
Investigation: Anqi Wang
Methodology: Anqi Wang, Xiaodong Liu
Resources: Anqi Wang
Software: Anqi Wang
Validation: Anqi Wang
Writing – original draft: Anqi Wang
Writing – review & editing: Xiaodong Liu, Zhi-Yong Yin

Abstract The direct radiative effect (DRE) of dust aerosols on the West African and East Asian monsoons is analyzed using the Community Atmosphere Model version 4 containing the dust aerosol parameterization module with and without the coupling of ocean-atmosphere processes, respectively. The atmospheric model (AM) and the ocean-atmosphere coupled model (CM) can both capture the major spatial characteristics of dust aerosols and summer monsoons over West Africa and East Asia. Our results show that the DREs on the West African (WASM) and East Asian summer monsoon (EASM) are more significant in the CM simulations compared to the AM simulations, causing the strengthening of the WASM and weakening of the EASM. The DRE of dust aerosols induces a negative radiative forcing leading to a surface cooling of the downstream ocean of the dust source region when the coupled ocean feedback is added. The distinct DRE of dust aerosols on the WASM and EASM are resulted from the relative locations of the ocean cooling regions to the respective monsoon regions. This study shows the importance of the coupled ocean-atmosphere processes in the DRE and its influences on the WASM and EASM systems.

1. Introduction

Dust aerosol is the major component of the tropospheric aerosols and also a vital factor of climate change through a variety of physical processes of interactions (Mahowald et al., 2014; Shao et al., 2011). The direct radiative effect (DRE) of dust aerosols can change the local atmospheric temperature by absorbing or scattering short-wave and long-wave radiations, and then affect the local and even global climate (Miller & Tegen, 1998; Tegen & Lacis, 1996). Dust can also change cloud albedo by participating in liquid- and ice-cloud physical processes, indirectly affect global and regional climate (DeMott et al., 2010; Huang et al., 2014; Ramanathan et al., 2001) or settle on snow and ice surface to change the surface albedo and further influence local and regional temperature and climate (Flanner et al., 2007; Hansen & Nazarenko, 2004; Qian et al., 2011; Skiles et al., 2018).

North Africa and East Asia have the highest frequency of dust storms in the world (Engelstaedter et al., 2003; Shao et al., 2013). The North African deserts (NAD) release approximately 1–1.5 billion tons of dust aerosols into the atmosphere each year, exceeding half of the total global emissions (Ginoux et al., 2004). The East Asian deserts (EAD) represented by Taklimakan and Gobi Deserts contribute more than 70% of the total dust aerosol emission in Asia (Zhang et al., 2003), and the dust aerosol concentration could reach 85 $\mu g/m^3$ in northwest China (Zhang et al., 2012). These large amounts of dust aerosol can change the regional or global climate through DRE.

In recent decades, many studies have used the atmospheric models (AMs), which refer to the models with prescribed sea surface temperature (SST) that does not respond to the variations of dust aerosols, to investigate the climate effects of radiation balance variations induced by dust aerosols over Africa and East Asia (Ginoux et al., 2004; Gu et al., 2016; Sun et al., 2012; Wu et al., 2013; Xie, Liu, Che, Xie, Wang, et al., 2018; Yue et al., 2009). Nicholson et al. (2000) pointed out that dust aerosols can affect climate through land-atmosphere interactions, resulting in precipitation decrease and leading to drought conditions in West Africa. However, Gu et al. (2006) simulated the DRE of dust aerosols using the atmospheric general circulation model developed by the University of California, Los Angeles (UCLA), and their results showed that the DRE of dust aerosols would lead to an increase in precipitation in North Africa. At the same time, dust aerosols of large particle sizes can suppress tropical convection and reduce precipitation in South China through decreasing the temperature

anomalies between this region and the middle to high latitudes. However, they put forth the opposite conclusion in their later study (Gu et al., 2016): the DRE of dust aerosols weakened precipitation in North Africa, while in East Asia, precipitation was strengthened in the north but weakened in the south. Solmon et al. (2012) used a regional climate model (RegCM) to simulate the DRE of dust aerosols in Sahel of West Africa, and their results showed that precipitation in this region presented a trend of decreasing over South Africa but increasing in North Africa. Sun et al. (2012) used the RegCM4 regional model to find that the concentration of dust aerosols was positively proportional to the amount of precipitation in the source region, but inversely proportional to precipitation in the downstream region because the induced cooling by dust aerosols led to a series of circulation anomalies. Xie, Liu, Che, Xie, Wang, et al. (2018) used the uncoupled Community Atmosphere Model version 4 containing the dust aerosol parameterization module to illustrate that the dust-radiation interactions weakened the dust-cycle in East Asia but strengthened it in North Africa. Wu et al. (2013) revealed that the influence of DREs on East Asian summer monsoon (EASM) and precipitation depended on the location of the monsoon precipitation band and its relative location to the dust source. As can be seen from all these results, the variations of DRE of dust aerosols over West Africa and East Asia and their impacts on climates have great uncertainties.

A large number of studies have shown that dust aerosols can be transported to oceans from dust source regions (Jickells et al., 2005; Knippertz & Todd, 2010; Tegen & Fung, 1994; Uno et al., 2009; Zhang et al., 1997), which may change the local/regional climate through the ocean-atmosphere interactions. Kim et al. (2010) showed that dust aerosols from the Sahara region of North Africa can be transported by atmospheric circulation to West Africa, the tropical Atlantic Ocean, the Caribbean Sea, and even Europe and the North Pacific. Dust aerosols emitted from the East Asian dust sources can be transported over the Pacific Ocean and even reaching Greenland and beyond over long distances (Bory et al., 2002; Jickells et al., 2005; Zhang et al., 1997). The dust aerosols transported from the dust source regions can modulate the energy balance of the ocean surface and cause cooling the SST through the DRE of the dust aerosols (Albani & Mahowald, 2019; Evan et al., 2008, 2009; Foltz & McPhaden, 2008). The coupled models are widely used to reveal the DRE of dust aerosols on the West African summer monsoon (WASM) (e.g., Balkanski et al., 2021; Jordan et al., 2018; Lau et al., 2009; Miller et al., 2004b, 2004a; Miller & Tegen, 1998; Solmon et al., 2012). Miller et al. (2004a) indicated that the DRE of dust aerosols strengthened the summer monsoon using the uncoupled model; however, the positive feedback was absent in the coupled modeling results due to the reduced evaporation. Jordan et al. (2018) revealed that the DRE of dust aerosols increased precipitation and the WASM in the AM simulation with fixed SST, while the adjustment of SST to the DRE resulted in reduced precipitation. Solmon et al. (2012) pointed out that the cooling of ocean could significantly decrease the enhanced precipitation induced by the DRE of dust aerosols over the Atlantic Ocean, but had no effect on the precipitation reduction over the Sahel region. Furthermore, many studies show that the absorption efficiency of dust aerosols is the cause of the differences in precipitation responses to the dust DRE (Miller et al., 2014; Perlwitz et al., 2001; Strong et al., 2015; Yoshioka et al., 2007). However, there is little research using the coupled ocean-atmospheric models to simulate the DRE of dust aerosols on the East Asian monsoon.

To sum up, the dust DREs simulated by models are very uncertain, and the models are very sensitive to the optical characteristics of dust particles. At the same time, it is difficult to fully describe the roles of dust DRE in the climate system only by using the AM experiments. Although previous studies (Balkanski et al., 2021; Jordan et al., 2018; Lau et al., 2009; Miller et al., 2004a, 2004b; Miller & Tegen, 1998; Solmon et al., 2012; Yoshioka et al., 2007) have noticed the effects of modification of the ocean on the climate responses to DRE, the dust DRE effects on global/regional precipitation remain elusive as summarized in Miller et al. (2014). Therefore, this study explores the influences of ocean-atmosphere interaction processes on the DRE of dust aerosols on the WASM and EASM systems, adjacent to the two largest dust sources in the world, by comparing the results of the AM simulations to those of the CM simulations by switching the dust radiative processes on and off in the models. This approach was used by Jordan et al. (2018) for the WASM, but has not been used for the EASM.

2. Experiment Design and Data Sets

2.1. Model Description and Numerical Experimental Design

The Community Climate System Model version 4 (CCSM4) uses flux couplers to connect general circulation climate models that include atmospheric, land surface, and ocean and sea ice processes. The Community

Atmospheric Model version 4 (CAM4) includes the dust emission, transport, dry and wet depositions, and radiative effects of dust aerosols (Neale et al., 2010). Here, we used the improved version of the CAM4 with a new Bulk Aerosol Model (BAM) parameterization (labeled as CAM4-BAM, Albani et al., 2014), including new dust size distributions (Kok, 2011) and dust optical properties from Yoshioka et al. (2007). The emitted dust size distributions were calculated based on the brittle fragmentation process, resulting in much more coarse dusts (Kok, 2011) compared to Mahowald et al. (2006). All the other specific settings are the same as in Xie, Liu, Che, Xie, Wang, et al. (2018).

The model also includes the response of snow and ice albedo to dust aerosol deposition (Flanner et al., 2007; Oleson et al., 2010; Shi et al., 2019; Xie, Liu, Che, Xie, Li, et al., 2018). Xie, Liu, Che, Xie, Li, et al. (2018) revealed that the snow darkening effect of dust aerosols had positive effects on the dust emissions over East Asia. Shi et al. (2019) illustrated that the DRE of dust aerosols strengthened the moisture convergence and rainfall over the Indian monsoon region through heating the low troposphere over the Arabian Peninsula.

In order to investigate the roles of the ocean-atmosphere coupling processes, two sets of experiments with (named as atmospheic model with dust DRE [AMD]) and atmospheic model with no dust DRE (AMN) were carried out using the AM component (Xie, Liu, Che, Xie, Wang, et al., 2018). Another two sets of experiments were conducted using the CM component, named as coupled model with dust DRE (CMD) and coupled model with no dust DRE (CMN), respectively (Albani & Mahowald, 2019). Thus, the differences of AMD-AMN and CMD-CMN should reflect the DRE of dust aerosols in the AM and CM simulations, respectively, and the comparisons between the two groups can illustrate the influences of the ocean-atmosphere coupling processes on the DRE of dust aerosols. We use an identical experimental design but different models from Jordan et al. (2018). For the AM experiments, both the AMD and AMN experiments were run for 21 years, and the average results of the last 15 years were taken for further analyses. For the AM experiments, the monthly mean SST for the year 2000 was used to force the atmosphere, while the SST was calculated and interacted synchronously with the atmosphere in both the CMD and CMN experiments. Considering that the response of atmospheric circulation to ocean temperature change is relatively slow, the CMD and CMN experiments were run for 60 years, and the average of the last 30 years was taken for the following analysis.

2.2. Data Sets

In order to verify the model simulation results and conduct comparative analysis, atmospheric, and dust data from the Modern-Era Retrospective analysis for Research and Applications, version 2 (MERRA-2) reanalysis and gridded precipitation data from the Global Precipitation Climatology Project (GPCP) are used. The MERRA-2 reanalysis was developed by NASA's Global Model and Assimilation Office. The data assimilation process has been improved based on the AM and the grids statistical analysis scheme in the Goddard Earth Observation System (Randles et al., 2013). As a reanalysis data set, MERRA-2 not only provides various meteorological parameters (such as wind, temperature, pressure, and humidity, etc.), but also the dust optical depth (DOD) corrected using the Advanced Very High-Resolution Radiometer (AVHRR), Moderate-resolution Imaging Spectroradiometer (MODIS), Aerosol Robotic Network (AERONET), and Multi-angle Imaging Spectro Radiometer (MISR) data from ground and space remote sensing (Suarez et al., 2008). This data set covers the period from 1980 to the present, with a horizontal resolution of $0.625° \times 0.5°$. Data used in this study include 2000–2017 monthly mean emissions and dust aerosol extinction coefficients, 850 hPa meridional and zonal winds, and 700 hPa and 850 hPa geopotential heights (GPH).

The GPCP precipitation is a global gridded precipitation data set originally developed by the US National Oceanic and Atmospheric Administration (NOAA), which combines the gauge data, infrared data of geosynchronous orbit satellites, and the microwave data of low-earth orbit satellites (Adler et al., 2003). The Shepard's algorithm (Willmott et al., 1985) was used to interpolate the gauge precipitation data onto the spherical grid, which not only reduced the difficulties caused by the sparse distribution of stations in certain underdeveloped areas, but also enabled the global precipitation statistics to reach a unified standard, which were conducive to enhancing the scientific nature of the data. The data covers the period from January 1979 to the present, and the horizontal resolution is $2.5° \times 2.5°$. The precipitation data set used in this study is the monthly averages from 2000 to 2017.

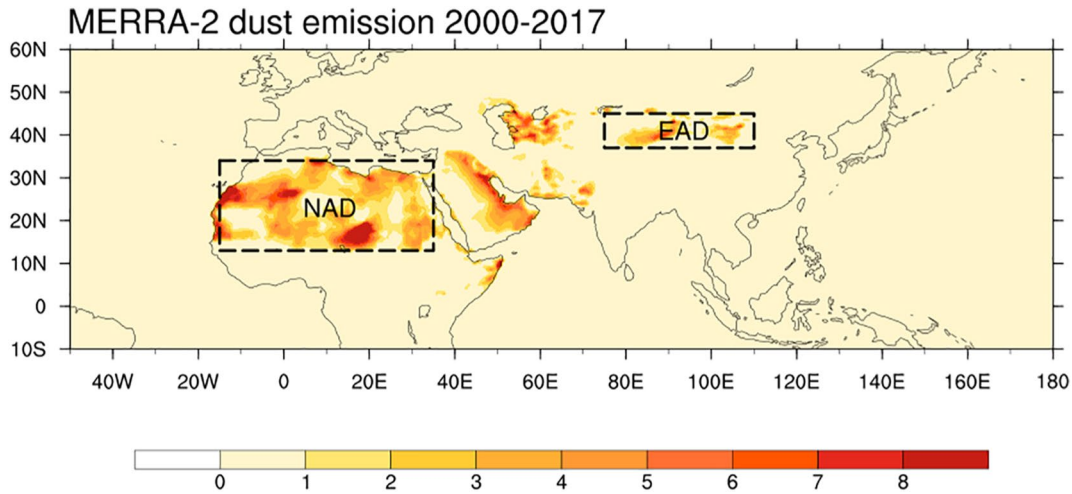

Figure 1. Distribution of annual dust emission flux (unit: 10^{-8} kg/m^2/s) averaged for 2000–2017 based on the Modern-Era Retrospective analysis for Research and Applications, version 2 (MERRA-2). The dashed boxes represent the North African deserts (NAD, 13°–34°N, −15° to 35°E) and East Asian deserts (EAD, 37°–45°N, 75°–110°E), respectively.

2.3. Study Regions

The NAD and EAD regions are the most important dust emission sources on Earth (Figure 1) and their dust aerosols influence the atmospheric circulation and precipitation of the downstream regions through the DRE (Sun et al., 2012; Wu et al., 2013). Note that comparisons between three reanalysis products revealed that the DOD has much uncertainty over Caribbean and tropical North Atlantic (Xian et al., 2020). However, previous studies have shown that the dust aerosol variables produced by the MERRA-2 reanalysis can very well reflect the dust activities over North Africa and East Asia. For example, Jordan et al. (2020) used the MERRA-2 reanalysis data sets to evaluate the spatial and temporal distributions of DOD in North Africa with a fully coupled meteorology-land-aerosol model, and Sun et al. (2020) compared and analyzed the Cloud-Aerosol Lidar and Infrared Pathfinder Satellite Observation (CALIPSO) satellite data against the MERRA-2 reanalysis data on the annual cycle of dust column concentration in different source regions in Asia, although the MERRA-2 values were higher than those of the satellite observations. Here, we use the DOD data obtained from MERRA-2 for the purpose of validation of the simulation results in this study.

The NAD and EAD regions can be clearly seen in the MERRA-2 annual average dust emissions flux distribution map during 2000–2017 (Figure 1). From the percent of average seasonal dust emissions in these two regions (Table 1), it can be seen that the dust emissions are highest in summer for NAD, but highest in spring for EAD, which are also consistent with previous studies (e.g., Gkikas et al., 2021; Kok et al., 2021; Lee et al., 2006). Therefore, this study focuses on the simulation results of spring and summer in the NAD and EAD regions.

Table 1
Percent of Spring (MAM), Summer (JJA), Autumn (SON) and Winter (DJF) Dust Emissions to the Annual Total Amounts Averaged for 2000–2017 in the Source Regions of North Africa Deserts (NAD) and East Asia Deserts (EAD) Based on the Modern-Era Retrospective Analysis for Research and Applications, Version 2 Reanalysis (Unit: %)

	MAM	JJA	SON	DJF
NAD	31.01	33.20	21.43	14.37
EAD	36.57	29.67	20.28	13.48

3. Evaluation of Simulation Results

The DOD, 850 hPa wind, GPH, and precipitation from the AM and CM simulations are compared with the corresponding MERRA-2 data. Figure 2 confirms that the highest DOD values in spring and summer are within the NAD and EAD regions. Over North Africa, the highest DOD values in the Sahara Desert and its surroundings are mainly concentrated in summer and can spread to the Atlantic Ocean in 5°–25°N (Figures 2d–2f). Dust activities in East Asia are mainly concentrated in the Taklimakan Desert and the Gobi region in spring, and can spread eastward to Japan, South Korea, and eastern Siberia, and even reach the north-central Pacific Ocean (Figures 2a–2c). The same results can be seen from both the AM and CM simulations as the geographical locations and diffusion gradients of the maximum DOD are

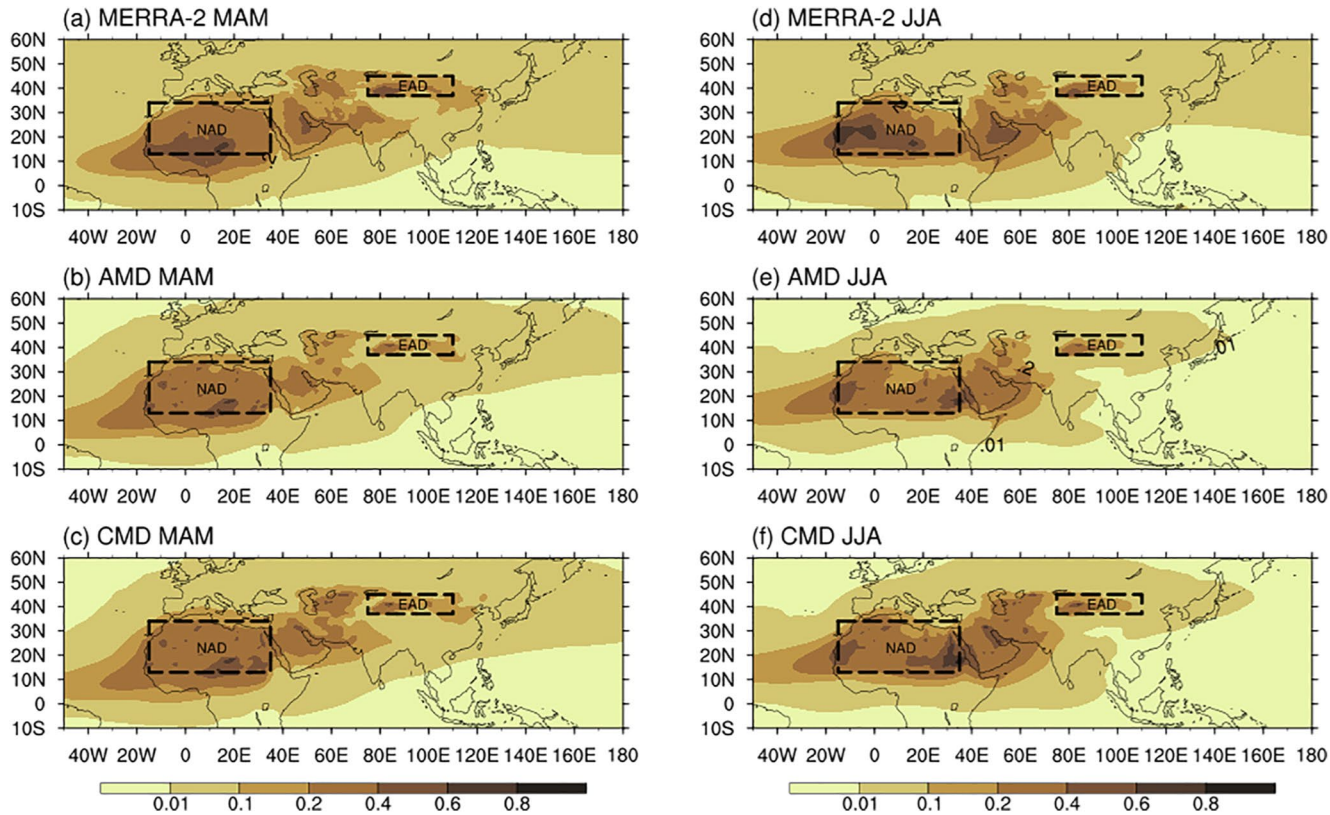

Figure 2. Average dust optical depth distributions of dust aerosols obtained by the reanalysis and simulations in spring (a–c) and summer (d–f). (a and d) Modern-Era Retrospective analysis for Research and Applications, version 2 (MERRA-2) reanalysis data; (b, e) Atmospheric model simulation; (c and f) Coupled model simulation. Dashed boxes indicate the same regions as shown in Figure 1.

consistent with the MERRA-2 data, which reflects that the characteristics of dust activities simulated by the models are realistic.

Not only can the simulation results correctly reflect the spatial distributions of dust aerosols, but also reproduce their annual cycle characteristics fairly well (Figure 3). The annual cycle characteristics of DOD over the NAD and EAD regions simulated by these two models are basically consistent with the MERRA-2 data. For NAD, high DOD values occur from March to August, but the highest values are found during May–June, while the seasonal mean results (Table 1) show that the highest value is in summer, followed by spring. In contrast, for EAD, the highest values occur in spring (April–May), followed by summer (also see Table 1). Figure S2 in Supporting Information S1 shows the highest values in the lower troposphere over NAD (Figure S2a in Supporting Information S1) and over EAD (Figure S2b in Supporting Information S1), respectively. It shows that the dust layer exists mainly in the lower troposphere. As shown in Table 2, the regionally averaged DOD differences between the MERRA-2 and AMD DOD are all larger than those between the MERRA-2 and CMD DOD. Also, as the indicators of how well the simulated DOD values match the MERRA-2 DOD values, spatial correlation coefficient (R) and root mean squared error (RMSE) values between the simulated and observed DOD fields are also calculated. The results simulated by CMD have a greater R and a smaller RMSE compared with the MERRA-2 data than those from the AMD simulation. Therefore, we conclude that the CM simulated DOD values match better to the observed DOD values than the AM simulation.

The summer monsoon is often characterized by the winds on 850 hPa both in the WASM and EASM regions (Jordan et al., 2018; Lau et al., 2009; Xie et al., 2016). Therefore, we selected the 850 hPa wind and GPH to evaluate the model in summer. Over EAD, the Taklamakan Desert is surrounded by mountains over 3 km above sea level and dusts can be transported at higher levels in spring when the region is dominated by the westerly circulation (Shao et al., 2011). Hence, we choose the 700 hPa wind and GPH to evaluate the simulated results in spring. The comparison between the MERRA-2 and simulated wind and geopotential height fields at 700 hPa in spring

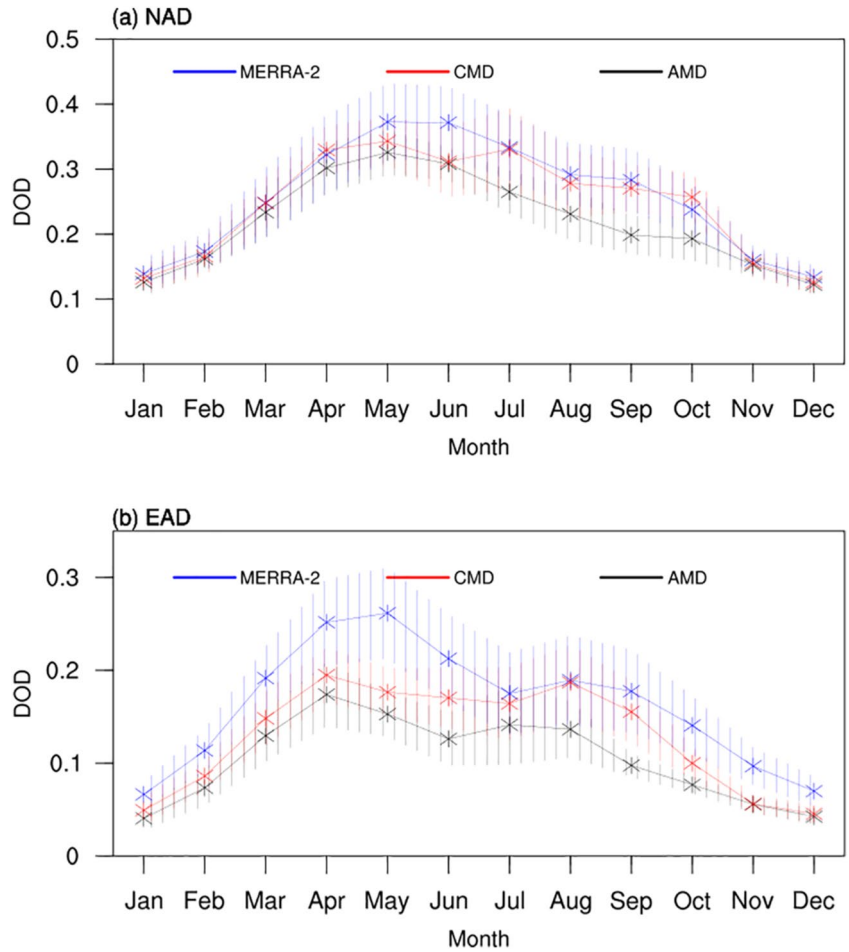

Figure 3. Annual cycles of climatological mean dust optical depth (DOD) of (a) the North African deserts (NAD) and (b) East Asian deserts (EAD) obtained by Modern-Era Retrospective analysis for Research and Applications, version 2 (MERRA-2) and simulations. The blue, red, and black lines represent MERRA-2, the coupled model simulation, and the atmospheric model simulation, respectively. Vertical lines represent the standard deviation of DOD.

Table 2
The Regionally Averaged Dust Optical Depth (DOD) Difference (MERRA-2-atmospheic model with dust DRE [AMD] or MERRA-2-coupled model with dust DRE [CMD]), Spatial Correlation Coefficient (R), and Root Mean Squared Error (RMSE) Between Modern-Era Retrospective Analysis for Research and Applications, Version 2 (MERRA-2) and Simulated Results for MAM and JJA in West African Summer Monsoon (WASM) and East Asian Summer Monsoon (EASM) Regions, Respectively

		WASM	WASM	EASM	EASM
DOD		MAM	JJA	MAM	JJA
MERRA-2 and AMD	Difference	0.04	0.07	0.08	0.06
	R	0.70	0.58	0.72	0.72
	RMSE	0.08	0.13	0.113	0.07
MERRA-2 and CMD	Difference	0.02	0.03	0.06	0.03
	R	0.79	0.67	0.74	0.88
	RMSE	0.07	0.12	0.09	0.06

and those at 850 hPa in summer show that both the AM and CM simulations can accurately replicate the westerly circulation in the mid- to high-latitudes in spring, the easterly circulation in the low latitudes, and the positions of the subtropical highs over the Atlantic Ocean and Pacific Ocean in summer, although the simulated values of wind speed and the central strength of the subtropical highs are relatively too high (Figure 4). The distribution patterns of the 700 hPa wind and GPH in spring show that the center of the high pressure over NAD is located between the mid-latitude westerlies and the low-latitude easterly circulation. In the meantime, the westerly winds are prevailing over EAD until they converge with the southwesterly airflow over the Pacific Ocean near 30°N in eastern China. This pattern is conducive to the dust aerosol transport from the source regions to the downstream Pacific Ocean (Figures 4a–4c). For East Asia, the highest dust emission occurs in spring, and dust aerosols are transported to the downstream through the mid- and lower-tropospheric circulations. Therefore, we mainly examine the atmospheric circulation at 700 hPa in spring, while for the summer monsoon, we focus on the circulation at 850 hPa. In summer, the North African high is seated over the Sahara Desert, and the northeasterly airflow and the cross-equatorial southeasterly airflow converge over the Atlantic Ocean near

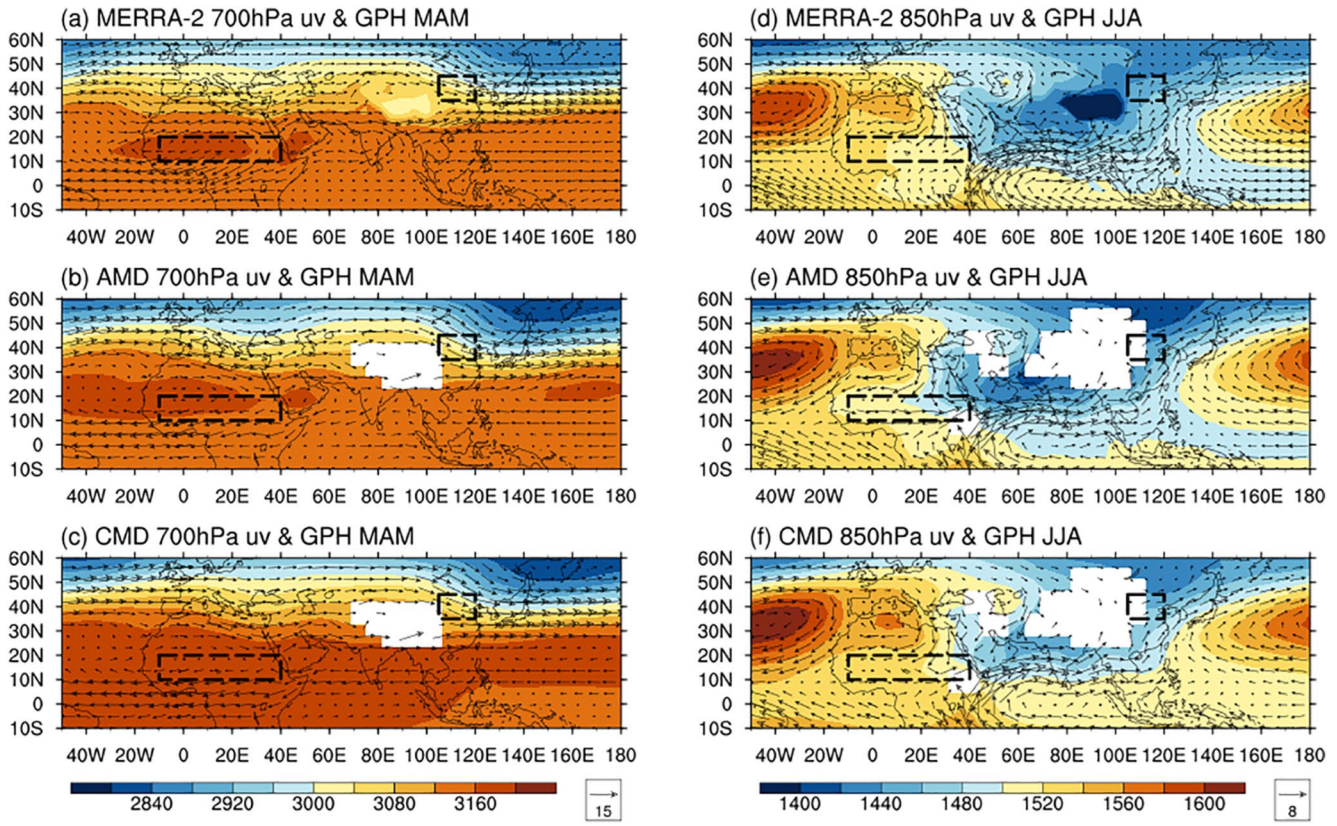

Figure 4. Modern-Era Retrospective analysis for Research and Applications, version 2 (MERRA-2) and simulated mean wind vector (unit: m/s) and geopotential height (unit: gpm) fields at 700 hPa in spring (a–c) and those at 850 hPa in summer (d–f). (a and d) MERRA-2; (b and e) Atmospheric model simulation; (c and f) Coupled model simulation. The dash-line boxes indicate the West African summer monsoon (WASM) (10°–20°N, −10° to 40°E) and East Asian summer monsoon (EASM) regions (35°–45°N, 105°–120°E) as defined in the text.

10°N, forming the equatorial easterlies. At the same time, the westerlies known as the WASM (Lau et al., 2009) dominate over the North African continent at 5°–15°N (Figures 4d–4f). As shown in Table 3, the differences for U, V, and GPH between the MERRA-2 data and AMD simulation are all larger than those between the MERRA-2 data and CMD simulation. Also, the results simulated by CMD have greater values of *R* and smaller values of RMSE compared with the MERRA-2 data for most situations than those of the AMD results. The above comparisons of the modeling results show that the CM simulation results in the WASM and EASM regions match better with the MERRA-2 reanalysis data than the AM results during the summer monsoon.

The comparative analyses of the simulated and observed precipitation distributions in spring and summer show that both the AM and CM simulations can accurately reflect the spatial distributions and seasonal variations of precipitation over West Africa and East Asia (Figure 5). In spring, the main rainfall region in Africa is found along the equator, while for Asia, it is mainly seen along the western margin of the Pacific, and there are also patches of high rainfall areas in the southeast coast of China, Southeast Asia, and southern Japan (Figures 5a–5c). In summer, precipitation increases significantly in both the WASM and EASM regions (including South Asia) (Figures 5d–5f). As shown in Table 4, the absolute value of the precipitation difference between the GPCP data and CMD results is smaller, with greater *R* and smaller RMSE values, than those between the GPCP and AMD values.

In short, the spatial and temporal variation patterns of the DOD, atmospheric circulation, and precipitation simulated by the AMD and CMD experiments are all realistic and reliable. However, the CM results match better to the reanalysis values compared to the AM results during the summer monsoon season.

Table 3
Difference (MERRA-2-atmospheic model with dust DRE [AMD] and MERRA-2-coupled model with dust DRE [CMD]), R (Spatial Pattern Correlation), and Root Mean Squared Error (RMSE) Between Modern-Era Retrospective Analysis for Research and Applications, Version 2 (MERRA-2) and Simulated Results for 700 hPa (MAM) and 850 hPa (JJA) U, V, geopotential height (GPH) in West African Summer Monsoon (WASM) and East Asian Summer Monsoon (EASM) Regions, Respectively

			WASM	WASM	EASM	EASM
			MAM	JJA	MAM	JJA
U	MERRA-2 and AMD	Difference	1.91	−4.86	−0.86	−0.41
		R	0.93	0.84	0.78	0.74
		RMSE	2.05	5.46	1.38	0.93
	MERRA-2 and CMD	Difference	1.13	−1.23	−1.02	−0.82
		R	0.94	0.89	0.94	0.65
		RMSE	1.42	2.26	1.19	1.11
V	MERRA-2 and AMD	Difference	−0.23	−0.03	1.92	−1.51
		R	0.79	0.69	0.84	0.72
		RMSE	1.10	1.77	2.04	1.68
	MERRA-2 and CMD	Difference	−0.58	0.47	1.49	−0.01
		R	0.71	0.84	0.88	0.74
		RMSE	0.72	1.35	1.61	0.56
GPH	MERRA-2 and AMD	Difference	−0.44	11.69	8.53	7.69
		R	0.71	0.88	0.98	0.96
		RMSE	3.51	16.8	11.29	8.55
	MERRA-2 and CMD	Difference	−21.4	−9.04	−16.1	−6.05
		R	0.70	0.98	0.99	0.97
		RMSE	20.36	7.42	6.78	6.03

4. Influences and Their Differences of the Dust DRE on the WASM and EASM

4.1. Influences of the Dust DRE on the WASM and EASM

The effects of the DRE of dust aerosols can be intuitively shown by the difference between the two experiments with and without the dust radiative feedbacks, that is, AMD minus AMN or CMD minus CMN. The WASM region (10°–20°N, −10° to 40°E) includes the Sahel and Southern Sahara from the west to the east of the African continent, meanwhile, precipitation in the region is sensitive to the WASM intensity (Lau et al., 2009). The prevailing westerly winds exist in the WASM region in summer in the lower troposphere (see Figure 4d), but the DRE of dust aerosols further strengthens the westerly winds in the monsoon region and its surrounding areas (Jordan et al., 2018), as indicated by the CM simulated 850 hPa wind field (Figure 6b) and the corresponding AM simulation result (Figure 6a). In the meantime, the DRE leads to the enhanced ascending air movement in the WASM represented by the 500 hPa vertical velocity (upward movement shown as blue shade in Figure 6), which is also widespread and statistically significant for the CM simulation, but not for the AM simulation. It is worth noting that our modeling results overestimate the westerly circulations but underestimate the meridional winds in the WASM region compared to the MERRA-2 reanalysis (Figures S1a and S1c in Supporting Information S1), which also play an important role to bring the humidity from the Gulf of Guinea. However, there is a significant positive anomaly of meridional winds induced by the dust DRE over the Gulf of Guinea in the CM results (Figure 6b), but not significant in the AM results (Figure 6a).

The EASM region (35°–45°N, 105°–120°E) includes the most part of northern China where the precipitation has been shown to be sensitive to both the climatic effects of aerosols and EASM intensity (Duan et al., 2014; Xie et al., 2016). Driving the EASM circulation, southerly winds prevail in the lower troposphere of the eastern part of East Asia in summer (Figure 4d). However, the DRE of dust produces northerly wind differences

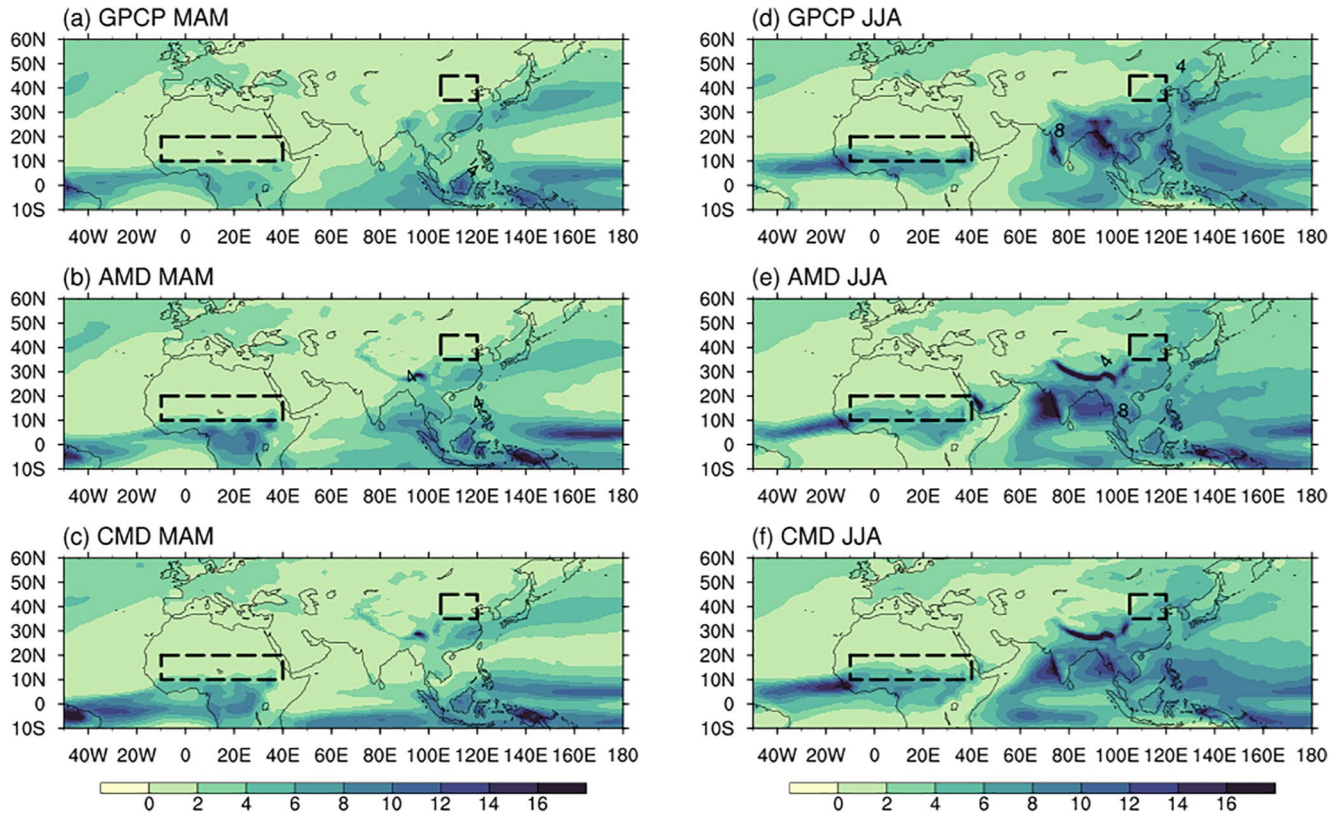

Figure 5. Observed and simulated mean precipitation (unit: mm/day) in spring (a–c) and in summer (d–f). (a and d) Global Precipitation Climatology Project (GPCP); (b and e) atmospheic model with dust DRE (AMD) simulation; (c and f) coupled model with dust DRE (CMD) simulation. Dashed boxes are the same as in Figure 4.

in the northern part of the East Asia monsoon region, leading to the weakened EASM as indicated by the CM simulation results (Figure 6d). At the same time, the DRE also weakens the 500 hPa upward movement over the EASM region. These responses are in contrast to those of the WASM, which are also more pronounced in the CM simulation (Figure 6b) than in the AM simulation.

In order to evaluate the modulating role of the ocean-atmosphere coupling processes on the DRE of dust aerosols, we compare the atmospheric responses to the DRE of dust aerosols in the CM and AM simulations by calculating the difference between CMD minus CMN and AMD minus AMN (Figures 6e and 6f) or [(CMD-CMN) – (AMD-AMN)]. As stated earlier, the first difference term (CMD-CMN) represents the dust DRE under the condition with ocean-atmosphere coupling processes, while the second difference term represents the dust DRE under the condition driven only by atmospheric dynamics. Therefore, the differences of wind fields (Figures 6e and 6f) represent the response to the dust DRE with the ocean-atmosphere interactions. The results show that the upwelling movements are more prominent in the westerly dominated WASM region, while the subsidence movements are more prominent in the EASM area accompanied by the anomalous northerly winds. It is thus clear that the ocean-atmosphere coupling processes strengthen the responses to the DRE in the WASM region and weaken the responses to the DRE in the EASM region.

The regional-scale atmospheric circulation patterns are directly related to the variations of monsoon precipitation. It is found that the dust DRE induced different circulation anomalies of the summer monsoons in West Africa and East Asia that can lead to the opposite trends of precipitation changes in these

Table 4
Precipitation Difference (GPCP-atmospheic model with dust DRE [AMD] and GPCP-coupled model with dust DRE [CMD]), R (Spatial Pattern Correlation), and Root Mean Squared Error (RMSE) Between Global Precipitation Climatology Project (GPCP) and Simulated Results for MAM and JJA in West African Summer Monsoon (WASM) and East Asian Summer Monsoon (EASM) Regions, Respectively. (Unit: mm/day)

		WASM	WASM	EASM	EASM
Precipitation		MAM	JJA	MAM	JJA
GPCP and AMD	Difference	−0.64	−0.61	−0.68	−1.60
	R	0.82	0.88	0.93	0.79
	RMSE	1.16	1.48	0.76	1.92
GPCP and CMD	Difference	−0.55	−0.01	−0.77	−1.59
	R	0.79	0.96	0.92	0.90
	RMSE	0.92	0.79	0.69	1.81

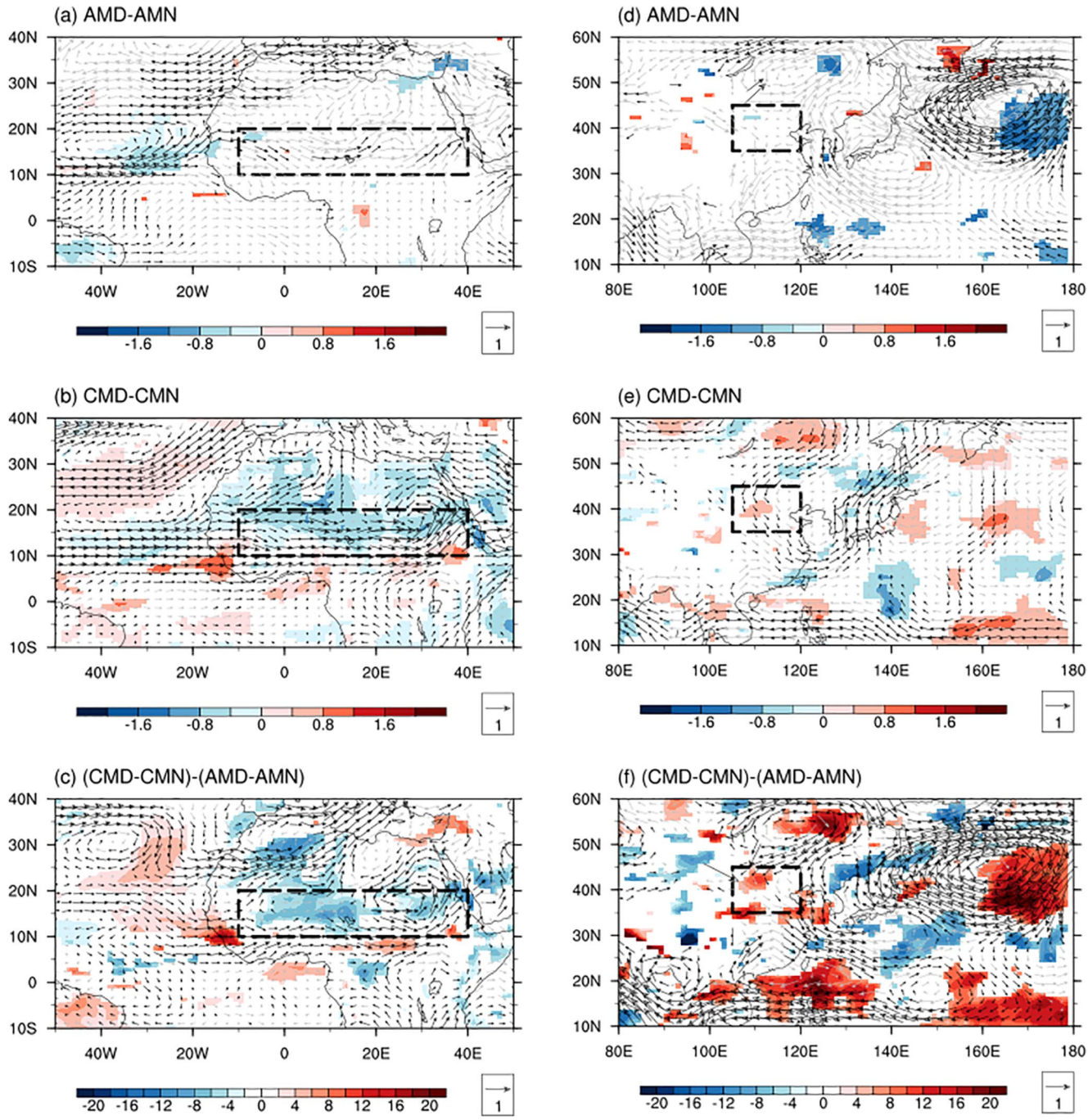

Figure 6. Changes in summer-mean 850 hPa horizontal wind (arrows, m/s) and 500 hPa vertical velocity (shaded, 10^{-2} Pa/s, blue color representing upward movement) fields induced by dust direct radiative effect simulated in the atmospheric model (AM) (a, b, atmospheic model with dust DRE [AMD]–atmospheic model with no dust DRE [AMN]), coupled model (CM) (c, d, coupled model with dust DRE [CMD]–coupled model with no dust DRE [CMN]), and their differences (e, f, CM-AM = (CMD-CMN) − (AMD-AMN)). Black (gray) arrows represent the wind vector differences statistically significant (insignificant) at 0.1 level. The changes in vertical velocity are shown only in areas passing 0.01 significance level. Dash boxes indicate the West African summer monsoon (WASM) (left panels) and East Asian summer monsoon (EASM) regions (right panels) same as in Figure 4.

two regions. Similar to the changes in wind patterns, precipitation in the WASM region does not change significantly under the AM simulation (Figure 7a), while precipitation in the northern margin of the EASM region increases (Figure 7b). Considering the large deviation between the precipitation simulated by the AM experiment and the observed values (Table 2), we mainly refer to the results of the CM experiment when analyzing

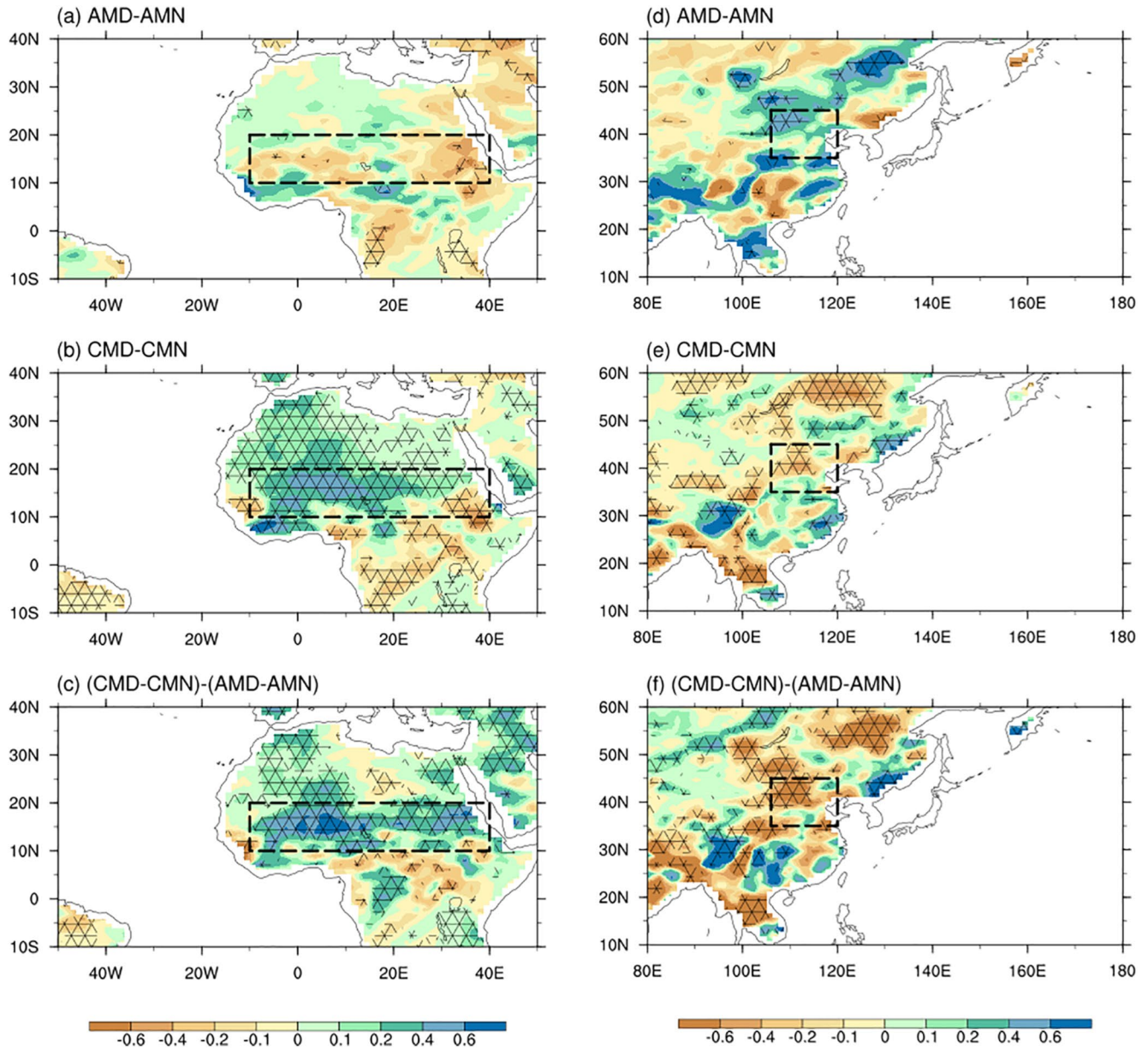

Figure 7. Changes in summer mean precipitation (shadow, mm/day) induced by dust direct radiative effect simulated by the atmospheric model (a and b atmospheic model with dust DRE [AMD]-atmospheic model with no dust DRE [AMN]), coupled model (c and d, coupled model with dust DRE [CMD]-coupled model with no dust DRE [CMN]) and (CMD-CMN) − (AMD-AMN). Black grids represent the value differences statistically significant (insignificant) at 0.1 level. Dash boxes indicate the West African summer monsoon (WASM) (left panels) and East Asian summer monsoon (EASM) regions (right panels) same as in Figure 4.

the influences of the DRE of dust aerosols on precipitation in the WASM and EASM regions. In the CMD experiment, the regional average precipitation in summer over the monsoon regions match better to the observed GPCP values than the AMD experiment (Table 2), and the DRE of dust aerosols causes a significant increase in the WASM precipitation (Figure 7c), but a decrease in the EASM precipitation (Figure 7d), and these changes are more significant than those in the AM simulations. We also use the difference between the CM and AM experiments, that is, [(CMD−CMN) − (AMD−AMN)] to represent the prominence of the roles played by the ocean-atmosphere coupling processes in modulating the DRE of dust aerosols. Large positive difference values represent amplified responses to the dust DRE by the ocean-atmosphere coupling, while large negative differences represent diminished responses to the dust DRE due to the coupling. According to Figures 7c and 7f,

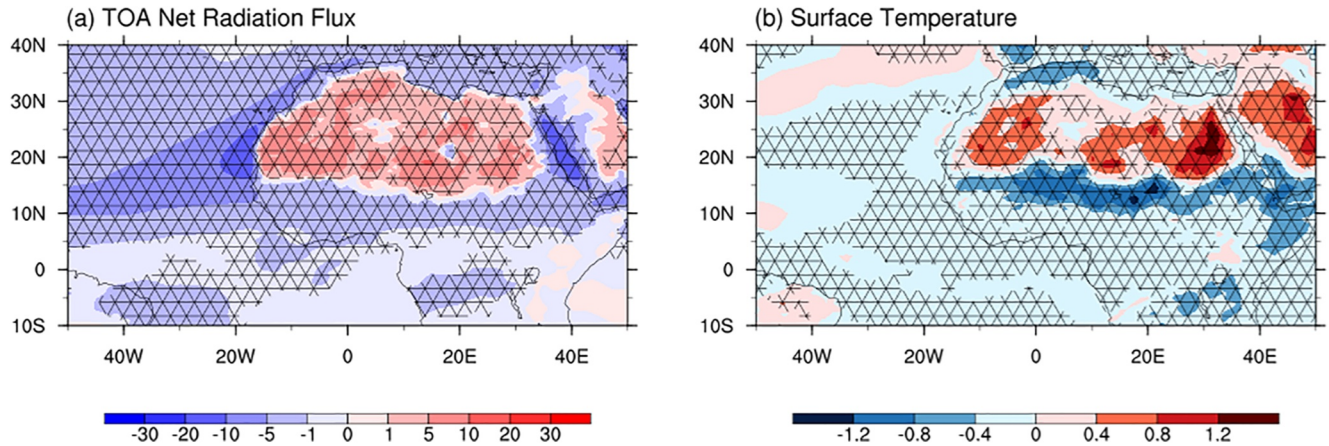

Figure 8. Changes in net radiation flux at the top of atmosphere (TOA) (a, atmospheic model with dust DRE-atmospheic model with no dust DRE, unit: W/m^2) and surface temperature (b, coupled model with dust DRE-coupled model with no dust DRE, unit: °C) induced by the direct radiative effect of dust aerosols over North Africa in summer. The black hatch lines represent the values passing the significance level of 0.1.

precipitation significantly increases in the WASM region while decreases in the EASM region with the effects of ocean-atmosphere coupling.

4.2. Physical Mechanisms for the Dust DRE on WASM

Since the CM experiment provides better matches to the reanalysis values (Section 3) than the AM experiment during the summer monsoon season, the following analyses are based on the differences between the CMD and CMN to examine the dust DRE on various physical processes. The DRE of dust aerosols can influence the regional and global climate by modulating the surface temperature through changing the radiation budget. Miller et al. (2014) pointed out that the changes in surface net radiation flux caused by DRE in regions frequently mixed by deep convection may not accurately represent the changes of temperature, which is true for both the WASM and EASM regions, and the changes of surface temperature should be calculated by using the net (short-wave + longwave) radiation flux at the top of atmosphere (TOA). In summer, dust aerosols not only exist over the source of NAD, but also spread over the Atlantic Ocean transported by the northeasterly airflow at the southeastern edge of the Atlantic subtropical high. Therefore, the DRE of dust aerosols simultaneously leads to the changes in the TOA net radiation flux over the NAD and its surrounding waters. Such changes of the TOA net radiation flux caused by the DRE of dust aerosol depend on the local surface albedos. The dust aerosols in areas with high surface albedos (such as the NAD) can reflect and reabsorb more short-wave radiation in the lower troposphere, resulting in a positive change of the TOA net radiation flux in this region, while in regions with low surface albedos (such as the Atlantic Ocean and the Sahel steppe) this produces a negative change in the net radiation flux of TOA (Figure 8a). This result has been verified in previous studies (Miller et al., 2004b; Takemura et al., 2009; Yoshioka et al., 2007). The CM simulation shows that the DRE of dust aerosols causes a positive change in the NAD land surface temperature, while a negative change in surface temperature occurs over the Sahel steppe region (south of the NAD) extending to the Gulf of Guinea and the Atlantic Ocean (Figure 8b), corresponding to the negative change in the TOA net radiation flux (Figure 8a).

These changes in surface temperature have an impact on the sea level pressure (SLP) field. The CM simulation shows that the increased surface temperature leads to a decrease in SLP in NAD and its surrounding waters. Over the Sahel steppe, however, there is an enhanced high SLP value due to the negative change in the surface temperature (Figure 9a). Although the regions with statistical significance above the 90% confidence level are mainly located in the North African continent, with the addition of the oceanographic feedback, the SLP pattern now contributes to the enhancement of the westerly circulation in the WASM region. Not only can the changes of surface air temperature of the land and oceans affect the SLP pattern, but these also further affect the GPH pattern in the lower troposphere across this region. The 850 hPa GPH become lower over NAD and its surrounding waters (Figure 9c), mainly due to the low-level heating induced by dust aerosols (Figure S3b in Supporting

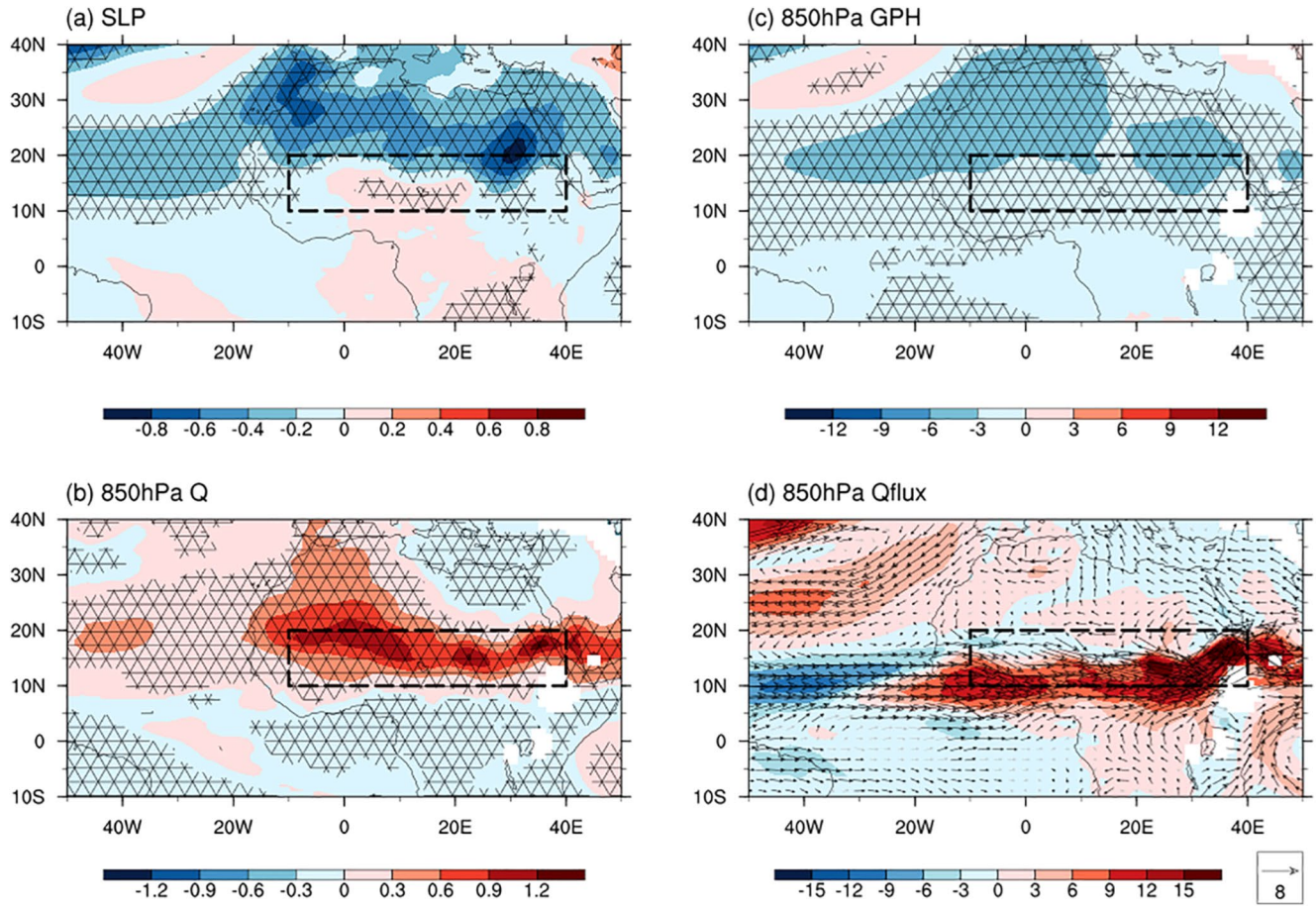

Figure 9. Changes (coupled model with dust DRE-coupled model with no dust DRE) in summer mean sea level pressure (SLP) values (a, SLP: hPa), 850 hPa geopotential height (b, GPH: gpm), 850 hPa specific humidity (c, Q: g/kg), and 850 hPa moisture flux (d, shaded, Qflux: g/(hPa m s)) fields induced by the direct radiative effect of dust aerosols over the West African summer monsoon (WASM) region (10°–20°N, −10° to 40°E). Black hatch lines (a–c) represent the values statistically significant at 0.1 level. Black (gray) arrows (d) represent the moisture flux vector differences statistically significant (insignificant) at 0.1 level. Dash boxes indicate the WASM region same as in Figure 4a.

Information S1). Additionally, the WASM region is located at the southern edge of the enhanced low-pressure zone, corresponding to the strengthening of the 850 hPa westerly winds (see Figure 6c). The dust DRE induced strengthening of the south-north gradient in the 850 hPa GPH field leads to enhance westerly airflow and transport of the Atlantic water vapor toward the inland, resulting in the increase of specific humidity and water vapor flux in the WASM region (Figures 9b and 9d), which is conducive to the increase of precipitation in the WASM region (Figure 7c). These results essentially conform to the findings by Jordan et al. (2018).

To sum up, the DRE of dust aerosols affects the net radiation flux of TOA, leading to the enhanced thermal difference between land and ocean over West Africa and its surrounding waters, which causes an enhanced westerly circulation and ascending motion over the WASM region, creating favorable conditions for precipitation from the perspective of atmospheric dynamics. At the same time, the enhanced westerly circulation is conducive to the water vapor transport from the tropical Atlantic Ocean entering the inland area, so that the DRE of dust aerosols also leads to the increase of specific humidity and water vapor flux in the lower troposphere, which increases the water vapor supply to the WASM region. Under the interactions of the above favorable dynamic and water vapor conditions, the WASM precipitation increases correspondingly.

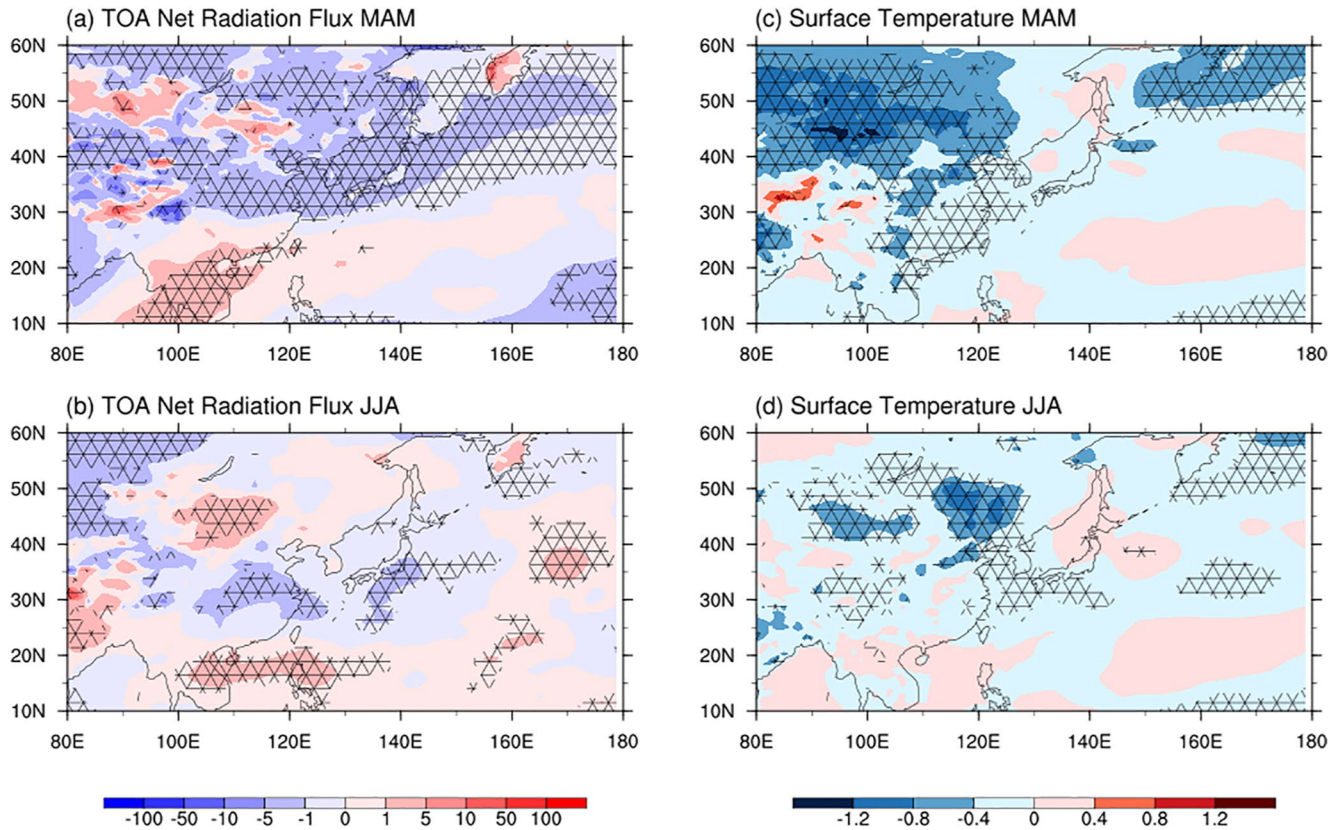

Figure 10. Changes in net radiation flux at the top of atmosphere (TOA) (a, atmospheic model with dust DRE-atmospheic model with no dust DRE, unit: W/m^2) and surface air temperature (b, coupled model with dust DRE-coupled model with no dust DRE, unit: °C) induced by the direct radiative effect of dust aerosols over North Africa in spring (a and c) and in summer (b and d). The black hatch lines represent the values passing the significance level of 0.1.

4.3. Physical Mechanisms for the Dust DRE on the EASM

Similar to the previous section on the responses of the WASM to the dust DRE, we use the differences of the CMD and CMN simulation results to further examine the responses of the EASM to the dust DRE. Since spring is the season with the highest dust aerosol emission and high levels of DOD continue during the summer months in the EAD region (Figure 3), the dust aerosol concentrations over the northwestern Pacific Ocean remain high from spring to summer (Figure 2), which significantly reduce the net radiation flux of TOA in the northwestern Pacific Ocean (Figure 10a). As a result, the corresponding changes in the spring SST are negative (Figure 10b) with a drop of 0.51°C over the region 50°–60°N and 150°–180°E (Figure 10b), and the cooling continues into the following summer (Figure 10d). On the other hand, the dust DRE induced changes in the summer net radiation flux of TOA are positive (regional average: +0.02 W/m^2) over the North Pacific Ocean (10°–50°N and 160°–180°E, Figure 10c), which should be conducive to the warming of SST in this region (Figure 10d). However, the changes in SST north of 30°N are mostly negative (regional average: −0.2°C) and statistically significant (Figure 10d). Considering the lower concentrations of dust aerosols over the Pacific Ocean in summer as compared to the spring level, its DRE should have limited influence on the changes of local/regional SST. Therefore, we conclude that the lowering of SST over the northwestern Pacific is mostly the result of the continuation of the spring condition due to the slow response and persistence of SST to net radiation flux variations. These results indicate that the DRE of dust aerosols during spring leads to the cooling of the overall temperature over the northwestern Pacific Ocean in both spring and summer.

The simulated dust DRE causes not only a marked cooling of SST (Figure 10d), but also significant rises in SLP and 850 hPa GPH over the northwestern Pacific Ocean, especially in 25°–45°N and 135°–160°E (Figures 11a and 11b). These changes reduce the zonal pressure gradient between the northwestern Pacific and EASM region, and produce anomalous northerly winds at 850 hPa (Figure 6d), thus leading to the weakening of the EASM.

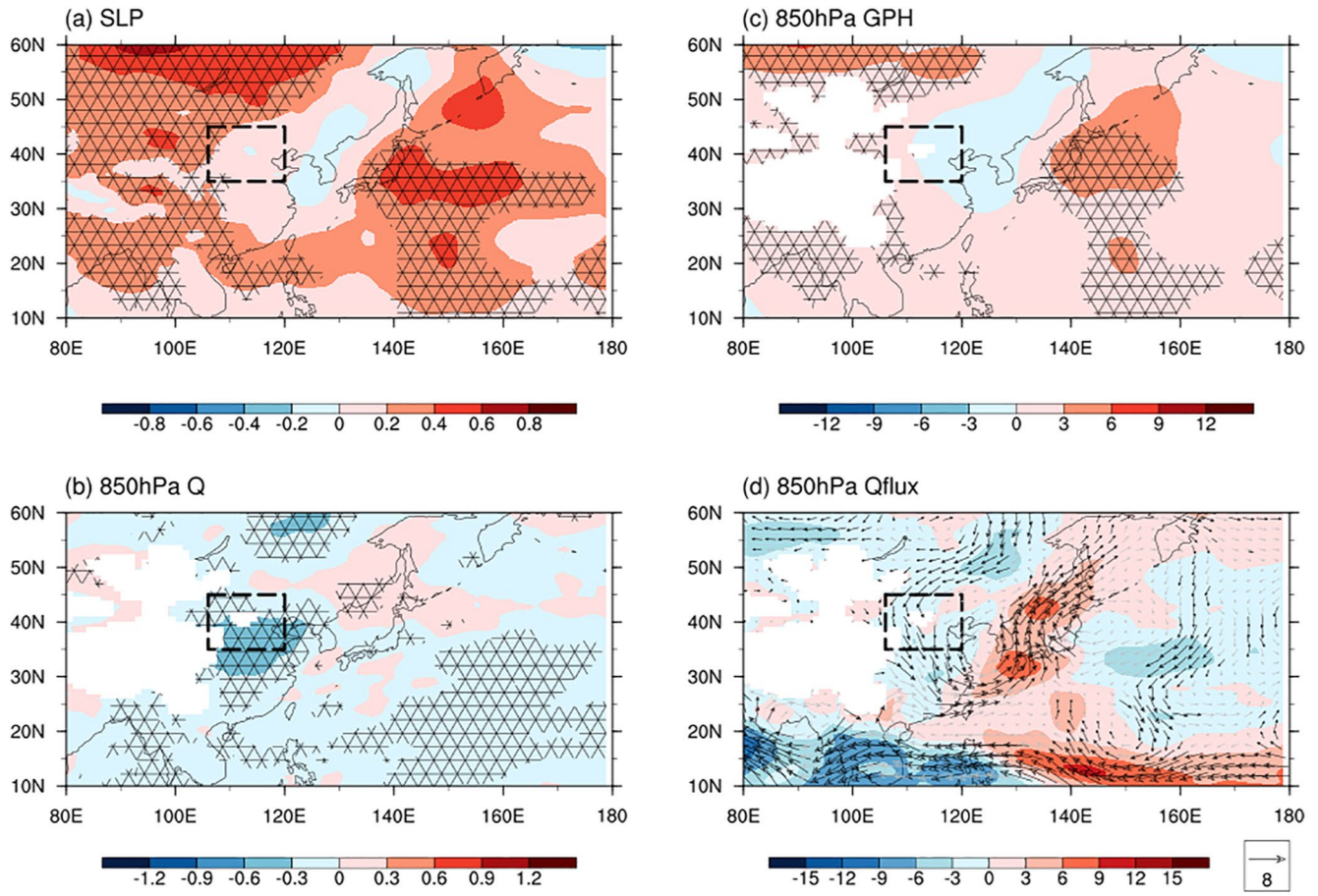

Figure 11. Changes (coupled model with dust DRE-coupled model with no dust DRE) in summer mean SLP values (a, SLP: hPa), 850 hPa geopotential height (b, GPH: gpm), 850 hPa specific humidity (c, Q: g/kg), and 850 hPa moisture flux (shaded, Qflux: g/(hPa m s)) fields induced by the direct radiative effect of dust aerosols over the West African summer monsoon (WASM) region (10°–20°N, −10° to 40°E). Black hatch lines (a–c) represent the values statistically significant at 0.1 level. Black (gray) arrows (d) represent the moisture flux vector differences statistically significant (insignificant) at 0.1 level. Dash boxes indicate the East Asian summer monsoon (EASM) same as in Figure 4d.

From the perspective of water vapor supply, the dust DRE causes significant decreases in the 850 hPa specific humidity and water vapor flux from south to north (Figures 11c and 11d), and thus restrains precipitation in the EASM region (Figure 7d).

4.4. Differences in Influences of the Dust DRE on WASM and EASM

The DRE of dust aerosols enhances the WASM but weakens the EASM. These distinctly different responses to the dust DRE between the WASM and EASM are the result from the relative location of the cooling oceans to the respective monsoon regions: the WASM region is located downwind of the prevailing winds near the surface of the Atlantic cooling area, and the temperature gradient between the NAD and Atlantic resulting in an enhanced south-north pressure gradient at the 850 hPa level (Figure 12a), producing westerly wind anomalies, which are in the same direction of the prevailing winds of the WASM and lead to the precipitation enhancement through bringing more water vapor flux to the monsoon region (Figure 9d). In the meantime, the EASM region is located in the upwind of the cooling region of the northwestern Pacific Ocean. Dust aerosols are transported from the EAD to the Pacific Ocean in spring, resulting in a decrease in SST that continues into the following summer. The cooling results in an anomalous high-pressure center over the northwestern Pacific with an anticyclonic flow pattern, which stimulates an anomalous low pressure with cyclonic flow pattern to the west (Figure 12b). Under the influence of the anomalous cyclonic circulation, the northerly wind anomalies in the western side

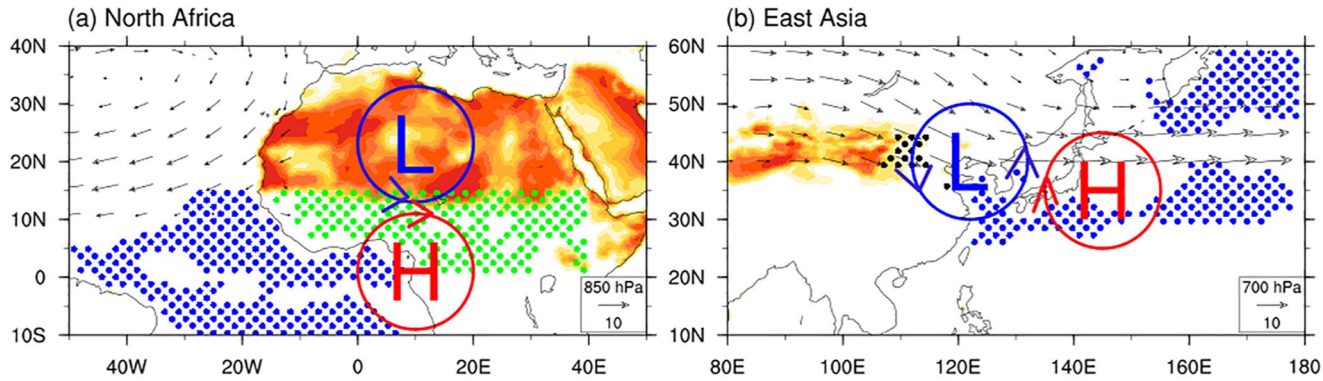

Figure 12. Schematic diagrams of the dust direct radiative effect induced anomalies of the summer monsoon circulation and precipitation over (a) North Africa and (b) East Asia. The shaded areas show dust source regions, where the airborne dust loading increases from yellow to red. The black arrows indicate the dust transport paths from the source to the oceans (a, 850 hPa wind in JJA; b, 700 hPa wind in MAM). The blue dots represent the areas of sea surface temperature cooling. The red (blue) circles represent anomalous anticyclonic circulations or high pressures (cyclonic circulations or low pressures) in the lower troposphere. The green (black) dots represent areas of precipitation increase (decrease).

of the cyclonic circulation are opposite to the prevailing southerly winds of the summer monsoon system over North China, resulting in the weakening of the EASM. In both cases, the ocean cooling caused by the DRE of dust aerosols leads to the rise of surface pressure and then affects the circulation and precipitation of the summer monsoons, which instead is not shown in the AM-only experiments. However, due to the distinct positions of the cooling areas relative to the monsoon regions, the final influences of DRE on the monsoons and summer precipitation are completely different for these two regions.

5. Summary and Discussion

The direct radiative effects (DRE) of dust aerosols on the West African and East Asian summer monsoons are compared and analyzed using the Community Atmosphere Model version 4 (CAM4) containing the dust aerosol parameterization module with and without the coupling of the ocean-atmosphere processes, respectively.

Our results show that the responses of the West African summer monsoon (WASM) and East Asian summer monsoon (EASM) to the dust DRE are more prominent when the ocean-atmosphere coupled processes are added: it significantly strengthens the WASM, same as seen in Jordan et al. (2018), but weakens the EASM. The distinct effects of dust aerosols on the WASM and EASM are resulted from the relative locations of the cooling ocean regions compared to the corresponding monsoon regions: the cooling ocean is upwind of the WASM region but downwind of the EASM region. This cooling ocean causes a south-north pressure gradient in North Africa, which enhances the westerly winds of the WASM. For the EASM, the cooling region generates an east-west pressure gradient, which strengthens the northerly winds and weakens the EASM.

The improved version of CAM4-BAM has been widely used to show the effects of dust aerosols on climate (Albani & Mahowald, 2019; Shi et al., 2019; Xie, Liu, Che, Xie, Li, et al., 2018; Xie, Liu, Che, Xie, Wang, et al., 2018). Albani and Mahowald (2019) used the same coupled CAM4-BAM to reveal the enhancement of WASM and precipitation induced by the DRE during the Last Glacial Maximum. Xie, Liu, Che, Xie, Wang, et al. (2018), Xie, Liu, Che, Xie, Li, et al. (2018) showed the DRE and the snow darkening effect of dust aerosols on dust emissions over East Asia using the uncoupled CAM4-BAM. Additionally, several other coupled models have been applied to investigate the dust-monsoon interactions (Jordan et al., 2018; Miller et al., 2004a, 2004b; Salmon et al., 2012; Strong et al., 2015). Jordan et al. (2018) proposed that the DRE of dust aerosols enhanced the WASM and precipitation in the western Sahel in an AM simulation with fixed SST, while the adjustment of SST to the DRE resulted in reduced precipitation. Miller et al. (2004a) revealed that the ocean cooling induced by dust DRE could weaken the Indian summer monsoon through comparing the coupled model results with the uncoupled ones and attributed these results to the evaporation decrease. However, our simulated results show that the WASM and precipitation in the monsoon region are significantly strengthened by the ocean cooling. Figure 13 shows the changes in the surface evaporation, surface temperature, and the wind speed at 10 m induced by the DRE of dust aerosols with the ocean-atmosphere coupling processes. Although the SST is reduced over the

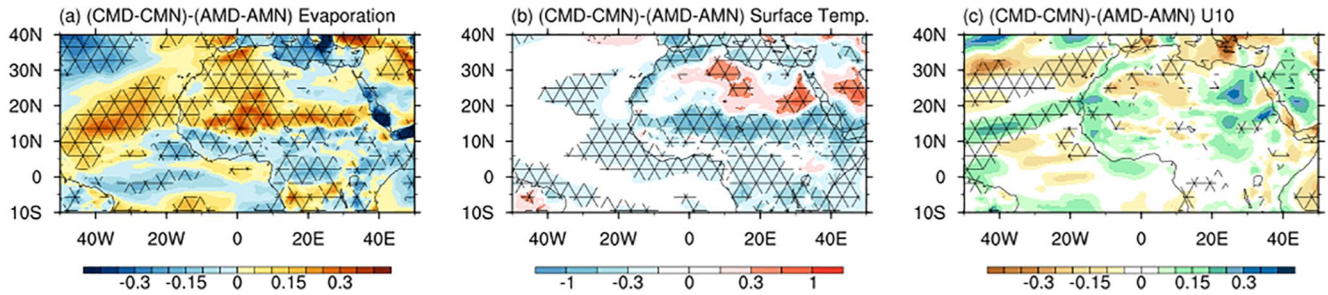

Figure 13. Changes in summer mean surface evaporation (a, unit: mm/day), surface temperature (b, unit: K) and the wind speed for 10 m (c, unit: m/s) induced by dust direct radiative effect simulated by the ocean-atmospheric coupled processes ((coupled model with dust DRE [CMD]-coupled model with no dust DRE [CMN]) − (atmospheic model with dust DRE [AMD]-atmospheic model with no dust DRE [AMN])). Black grids represent the value differences statistically significant at 0.1 level.

Atlantic Ocean, there is actually enhanced surface evaporation over this region (Figure 13a) due to the enhanced wind speeds (Figure 13c), which result in significant increases in specific humidity and moisture flux, and in turn the precipitation increases in the WASM region. Our results indicate that the role of ocean-atmosphere interactions increases the WASM through the enhanced ocean-land thermal gradient, which is opposite to Miller et al. (2004a) and Jordan et al. (2018). This difference may be accounted for by the absorption efficiency of dust aerosols assumed by the different studies, which mainly determines the monsoon strengthening or weakening (Balkanski et al., 2021; Miller et al., 2014; Perlwitz et al., 2001; Solmon et al., 2012; Strong et al., 2015; Yoshioka et al., 2007). Through sensitivity experiments of the dust absorption efficiency, previously studies have shown that the direction of precipitation change in the WASM region is strongly dependent on the dust absorption efficiency, where high (low) dust absorption can enhance (weaken) the WASM precipitation (Balkanski et al., 2021; Miller et al., 2004b; Strong et al., 2015). A number of GCMs underestimate coarse dusts and then the dust absorption efficiency (Kok, 2011). In this current study, we use an improved dust emissions size distribution with more coarse dusts and higher dust absorption efficiency (Albani et al., 2014; Kok, 2011), which explains the enhanced WASM and precipitation by the dust DRE in our results. On the other hand, high absorbing dust aerosols more significantly reduce the upper-ocean heat content energy and lower the SST through dynamical ocean responses compared with low absorbing dusts (Strong et al., 2015), which may affect the ocean-land thermal gradient and monsoonal circulations. Hence, ocean-feedbacks due to different absorption efficiencies also play a nonnegligible role in enhancing the WASM.

One limitation of this study is that we only considered the DRE of dust aerosols, and did not consider the indirect effects, such as dust aerosol-ice cloud interactions. For example, Sagoo and Storelvmo (2017) used CAM version 5.1 to study the dust-ice cloud interaction, and their results showed that the dust aerosols could increase the number of ice nucleating particles in the mixed-phase clouds and reduce the ice crystal size. Such effects thereby prolonged the life of the clouds that reflected more shortwave solar radiation, weakened the ground net radiation flux, and decreased the surface temperature. This current research does not consider this effect, which may cause an underestimate of the impact of dust aerosols on climate. Future studies can take into account the interactions between dust and ice clouds, so as to more accurately evaluate the impact of dust aerosols on climate. There is also the need to examine the SST response to DRE and the underlying ocean mixed layer dynamics in future investigations.

Data Availability Statement

All reanalysis data sets used in this research are openly available. The MERRA-2 data set can be downloaded from the Goddard Earth Science Data and Information Service Center (https://disc.gsfc.nasa.gov/). All precipitation data sets are available in the NCAR Climate Data Guide website (https://climatedataguide.ucar.edu/climate-data/gpcp-monthly-global-precipitation-climatology-project). All the simulated data about the Atmospheric Model and the Ocean-Atmosphere Coupled Model can be obtained on East Asian Paleoenvironmental Science Database (http://paleodata.ieecas.cn/FrmDataInfo.aspx?id=e0acd5cf-2176-42a2-9367-32e4cf99401c).

Acknowledgments
This research was jointly supported by the National Natural Science Foundation of China (Grant No. 41991254) and the Strategic Priority Research Program of Chinese Academy of Sciences (Grant Nos. XDB40030100 and XDA20070103). Xie X. is supported by the National Natural Science Foundation of China (Grant No. 42175059) and the CAS "Light of West China" program (Grant No. XAB2019A02).

References

Adler, R. F., Huffman, G. J., Chang, A., Ferraro, R., Xie, P., Janowiak, J., et al. (2003). The version 2.1 global precipitation Climatology Project (GPCP) monthly precipitation analysis (1979-present). *Journal of Hydrometeorology*, *4*, 1147–1167. https://doi.org/10.1175/1525-7541(2003)004<1147:TVGPCP>2.0.CO;2

Albani, S., & Mahowald, N. M. (2019). Paleodust insights into dust impacts on climate. *Journal of Climate*, *32*(22), 7897–7913. https://doi.org/10.1175/JCLI-D-18-0742.1

Albani, S., Mahowald, N. M., Perry, A. T., Scanza, R. A., Zender, C. S., Heavens, N. G., et al. (2014). Improved dust representation in the community atmosphere model. *Journal of Advances in Modeling Earth Systems*, *6*, 541–570. https://doi.org/10.1002/2013MS000279

Balkanski, Y., Bonnet, R., Boucher, O., Checa-Garcia, R. C., & Servonnat, J. (2021). Better representation of dust can improve climate models with too weak an African monsoon. *Atmospheric Chemistry and Physics*, *21*(14), 11423–11435. https://doi.org/10.5194/acp-21-11423-2021

Bory, J. M., Biscaye, P. E., Svensson, A., & Grousset, F. E. (2002). Seasonal variability in the origin of recent atmospheric mineral dust at NorthGRIP, Greenland. *Earth and Planetary Science Letters*, *196*(3–4), 123–134. https://doi.org/10.1016/S0012-821X(01)00609-4

DeMott, P. J., Prenni, A. J., Liu, X., Kreidenweis, S. M., Petters, M. D., Twohy, C. H., et al. (2010). Predicting global atmospheric ice nuclei distributions and their impacts on climate. *Proceedings of the National Academy of Sciences of the United States of America*, *107*(25), 11217–11222. https://doi.org/10.1073/pnas.0910818107

Duan, Y. W., Zhu, K. Y., Ma, Z. G., & Yang, Q. (2014). Characteristics of precipitation concentration index (PCI) variations and monthly distribution of annual precipitation in China. *Chinese Journal of Atmospheric Sciences*, *38*(6), 1124–1136. https://doi.org/10.3878/j.issn.1006-9895.1401.13267

Engelstaedter, S., Kohfeld, K. E., Tegen, I., & Harrison, S. P. (2003). Controls of dust emissions by vegetation and topographic depressions: An evaluation using dust storm frequency data. *Geophysical Research Letters*, *30*(6), 96. https://doi.org/10.1029/2002GL016471

Evan, A. T., Heidinger, A. K., Bennartz, R., Bennington, V., Mahowald, N. M., Corrada-Bravo, H., et al. (2008). Ocean temperature forcing by aerosols across the Atlantic tropical cyclone development region. *Geochemistry, Geophysics, Geosystems*, *9*(5), Q05V04. https://doi.org/10.1029/2007GC001774

Evan, A. T., Vimont, D. J., Heidinger, A. K., Kossin, J. P., & Bennartz, R. (2009). The role of aerosols in the evolution of tropical North Atlantic Ocean temperature anomalies. *Science*, *324*, 778–781. https://doi.org/10.1126/science.1167404

Flanner, M. G., Zender, C. S., Randerson, J. T., & Rasch, P. J. (2007). Present day climate forcing and response from black carbon in snow. *Journal of Geophysical Research*, *112*, D11202. https://doi.org/10.1029/2006JD008003

Foltz, G. R., & McPhaden, M. J. (2008). Trends in Saharan dust and tropical Atlantic climate during 1980–2006. *Geophysical Research Letters*, *35*, L20706. https://doi.org/10.1029/2008GL035042

Ginoux, P., Prospero, J., Torres, O., & Chin, M. (2004). Long-term simulation of global dust distribution with the GOCART model: Correlation with North Atlantic Oscillation. *Environmental Modelling & Software*, *19*(2), 113–128. https://doi.org/10.1016/s1364-8152(03)00114-2

Gkikas, A., Proestakis, E., Amiridis, V., Kazadzis, S., Di Tomaso, E., Tsekeri, A., et al. (2021). ModIs dust AeroSol (MIDAS): A global fine-resolution dust optical depth dataset. *Atmospheric Measurement Techniques*, *14*, 309–334. https://doi.org/10.5194/amt-14-309-2021

Gu, Y., Liou, K. N., Xue, Y., Mechoso, C. R., Li, W., & Luo, Y. (2006). Climatic effects of different aerosol types in China simulated by the UCLA general circulation model. *Journal of Geophysical Research*, *111*, D15201. https://doi.org/10.1029/2005jd006312

Gu, Y., Xue, Y., De Sales, F., & Liou, K. N. (2016). A GCM investigation of dust aerosol impact on the regional climate of North Africa and South/East Asia. *Climate Dynamics*, *46*, 2353–2370. https://doi.org/10.1007/s00382-015-2706-y

Hansen, J., & Nazarenko, L. (2004). Soot climate forcing via snow and ice albedos. *Proceedings of the National Academy of Sciences of the United States of America*, *101*, 423–428. https://doi.org/10.1073/pnas.2237157100

Huang, J., Wang, T., Wang, W., Li, Z., & Yan, H. (2014). Climate effects of dust aerosols over East Asian arid and semiarid regions. *Journal of Geophysical Research*, *119*, 11398–11416. https://doi.org/10.1002/2014JD021796

Jickells, T. D., An, Z., Andersen, K. K., Baker, A. R., Bergametti, G., Brooks, N., et al. (2005). Global iron connections between desert dust, ocean biogeochemistry, and climate. *Science*, *308*(5718), 67–71. https://doi.org/10.1126/science.1105959

Jordan, A. K., Gnanadesikan, A., & Zaitchik, B. F. (2018). Simulated dust aerosol impacts on Western Sahelian rainfall: Importance of ocean coupling. *Journal of Climate*, *31*(22), 9107–9124. https://doi.org/10.1175/jcli-d-17-0819.1

Jordan, A. K., Zaitchik, B. F., Gnanadesikan, A., Kim, D., & Badr, H. S. (2020). Strength of linkages between dust and circulation over North Africa: Results from a coupled modeling system with active dust. *Journal of Geophysical Research*, *125*, e2019JD030961. https://doi.org/10.1029/2019JD030961

Kim, K. M., Lau, W. K. M., Sud, Y. C., & Walker, G. K. (2010). Influence of aerosol-radiative forcings on the diurnal and seasonal cycles of rainfall over West Africa and Eastern Atlantic Ocean using GCM simulations. *Climate Dynamics*, *35*(1), 115–126. https://doi.org/10.1007/s00382-010-0750-1

Knippertz, P., & Todd, M. C. (2010). The central west Saharan dust hotspot and its relation to African easterly waves and extratropical disturbances. *Journal of Geophysical Research*, *115*, D12117. https://doi.org/10.1029/2009jd012819

Kok, J. F. (2011). A scaling theory for the size distribution of emitted dust aerosols suggests climate models underestimate the size of the global dust cycle. *Proceedings of the National Academy of Sciences of the United States of America*, *108*, 1016–1021. https://doi.org/10.1073/pnas.1014798108

Kok, J. F., Adebiyi, A. A., Albani, S., Balkanski, Y., Checa-Garcia, R., Chin, M., et al. (2021). Improved representation of the global dust cycle using observational constraints on dust properties and abundance. *Atmospheric Chemistry and Physics*, *21*, 8127–8167. https://doi.org/10.5194/acp-21-8127-2021

Lau, K. M., Kim, K. M., Sud, Y. C., & Walker, G. K. (2009). A GCM study of the response of the atmospheric water cycle of West Africa and the Atlantic to Saharan dust radiative forcing. *Annales Geophysicae*, *27*(10), 4023–4037. https://doi.org/10.5194/angeo-27-4023-2009

Lee, H. N., Igarashi, Y., Chiba, M., Aoyama, M., Hirose, K., & Tanaka, T. (2006). Global model simulations of the transport of Asian and Sahara dust: Total deposition of dust mass in Japan. *Water, Air, and Soil Pollution*, *169*, 137–166. https://doi.org/10.1007/s11270-006-1895-8

Mahowald, N. M., Albani, S., Kok, J. F., Engelstaedter, S., Scanza, R., Ward, D. S., & Flanner, M. G. (2014). The size distribution of desert dust aerosols and its impact on the Earth system. *Aeolian Research*, *15*, 53–71. https://doi.org/10.1016/j.aeolia.2013.09.002

Mahowald, N. M., Muhs, D. R., Levis, S., Rasch, P. J., Yoshioka, M., Zender, C. S., & Luo, C. (2006). Change in atmospheric mineral aerosols in response to climate: Last glacial period, preindustrial, modern, and doubled carbon dioxide climates. *Journal of Geophysical Research*, *111*(D10), D10202. https://doi.org/10.1029/2005JD006653

Miller, R. L., Knippertz, P., Pérez, G. C., Perlwitz, J. P., & Tegen, I. (2014). Impact of dust radiative forcing upon climate. In *Mineral dust* (pp. 327–357). https://doi.org/10.1007/978-94-017-8978-3_13

Miller, R. L., Perlwitz, J., & Tegen, I. (2004a). Modeling Arabian dust mobilization during the Asian summer monsoon: The effect of prescribed versus calculated SST. *Geophysical Research Letters*, *31*, L22214. https://doi.org/10.1029/2004GL020669

Miller, R. L., Perlwitz, J., & Tegen, I. (2004b). Surface radiative forcing by soil dust aerosols and the hydrologic cycle. *Journal of Geophysical Research*, *109*, D04203. https://doi.org/10.1029/2003jd004085

Miller, R. L., & Tegen, I. (1998). Climate response to soil dust aerosols. *Journal of Climate*, *11*, 3247–3267. https://doi.org/10.1175/1520-0442(1998)011<3247:crtsda>2.0.co;2

Neale, R. B., Richter, J. H., Conley, A. J., Park, S., Lauritzen, P. H., Gettelman, A., et al. (2010). Description of the NCAR community atmosphere model (CAM 4.0). *NCAR Tech. Note NCAR/TN-485+ STR*, *1*(1), 1–12.

Nicholson, S. E., Somé, B., & Koné, B. (2000). An analysis of recent rainfall conditions in West Africa, including the rainy seasons of the 1997 El Niño and the 1998 La Niña years. *Journal of Climate*, *13*, 2628–2640. https://doi.org/10.1175/1520-0442(2000)013<2628:AAORRC>2.0.CO;2

Oleson, K. W., Lawrence, D. M., Bonan, G. B., Flanner, M. G., Kluzek, E., Lawrence, P. J., et al. (2010). *Technical description of version 4.0 of the community land model (CLM), NCAR tech*. National Center for Atmospheric Research. Note, TN-4781STR. https://doi.org/10.5065/D6FB50WZ

Perlwitz, J., Tegen, I., & Miller, R. L. (2001). Interactive soil dust aerosol model in the GISS GCM1. Sensitivity of the soil dust cycle to radiative properties of soil dust aerosols. *Journal of Geophysical Research*, *106*(16), 18167–18192. https://doi.org/10.1029/2000JD900668

Qian, Y., Flanner, M. G., Leung, L. R., & Wang, W. (2011). Sensitivity studies on the impacts of Tibetan Plateau snowpack pollution on the Asian hydrological cycle and monsoon climate. *Atmospheric Chemistry and Physics*, *11*, 1929–1948. https://doi.org/10.5194/acp-11-1929-2011

Ramanathan, V., Crutzen, P. J., Kiehl, J. T., & Rosenfeld, D. (2001). Aerosols, climate, and the hydrological cycle. *Science*, *294*, 2119–2124. https://doi.org/10.1126/science.1064034

Randles, C. A., Colarco, P. R., & Silva, A. D. (2013). Direct and semi-direct aerosol effects in the NASA GEOS-5 AGCM: Aerosol-climate interactions due to prognostic versus prescribed aerosols. *Journal of Geophysical Research*, *118*, 149–169. https://doi.org/10.1029/2012jd018388

Sagoo, N., & Storelvmo, T. (2017). Testing the sensitivity of past climates to the indirect effects of dust. *Geophysical Research Letters*, *44*, 5807–5817. https://doi.org/10.1002/2017gl072584

Shao, Y., Klose, M., & Wyrwoll, K. H. (2013). Recent global dust trend and connections to climate forcing. *Journal of Geophysical Research*, *118*, 11107–11118. https://doi.org/10.1002/jgrd.50836

Shao, Y., Wyrwoll, K. H., Chappell, A., Huang, J., Lin, Z., McTainsh, G. H., et al. (2011). Dust cycle: An emerging core theme in Earth system science. *Aeolian Research*, *2*, 181–204. https://doi.org/10.1016/j.aeolia.2011.02.001

Shi, Z., Xie, X., Li, X., Yang, L., Xie, X., Lei, J., et al. (2019). Snow-darkening versus direct radiative effects of mineral dust aerosol on the Indian summer monsoon onset: Role of temperature change over dust sources. *Atmospheric Chemistry and Physics*, *19*(3), 1605–1622. https://doi.org/10.5194/acp-19-1605-2019

Skiles, S. M., Flanner, M., Cook, J. M., Dumont, M., & Painter, T. H. (2018). Radiative forcing by light-absorbing particles in snow. *Nature Climate Change*, *8*, 964–971. https://doi.org/10.1038/s41558-018-0296-5

Solmon, F., Elguindi, N., & Mallet, M. (2012). Radiative and climatic effects of dust over West Africa, as simulated by a regional climate model. *Climate Research*, *52*, 97–113. https://doi.org/10.3354/cr01039

Strong, J. D. O., Vecchi, G. A., & Ginoux, P. (2015). The response of the tropical Atlantic and West African climate to Saharan dust in a fully coupled GCM. *Journal of Climate*, *28*(18), 7071–7092. https://doi.org/10.1175/jcli-d-14-00797.1

Suarez, M. J., Rienecker, M., Todling, R., Bacmeister, J., Takacs, L., Liu, H. C., et al. (2008). The GEOS-5 data assimilation system—Documentation of version 5.0.1, 5.1.0, and 5.2.0. *NASA Technical Report Series on Global Modeling and Data Assimilation*, *27*, 1–118.

Sun, H., Liu, X., & Wang, A. (2020). Seasonal and interannual variations of atmospheric dust aerosols in mid and low latitudes of Asia - A comparative study. *Atmosphere Research*, *24*, 105036. https://doi.org/10.1016/j.atmosres.2020.105036

Sun, H., Pan, Z., & Liu, X. (2012). Numerical simulation of spatial temporal distribution of dust aerosol and its direct radiative effects on East Asian climate. *Journal of Geophysical Research*, *117*(D13), D13206. https://doi.org/10.1029/2011JD017219

Takemura, T., Egashira, M., Matsuzawa, K., Ichijo, H., O'ishi, R., & Abe-Ouchi, A. (2009). A simulation of the global distribution and radiative forcing of soil dust aerosols at the Last Glacial Maximum. *Atmospheric Chemistry and Physics*, *9*, 3061–3073. https://doi.org/10.5194/acp-9-3061-2009

Tegen, I., & Fung, I. (1994). Modeling of mineral dust in the atmosphere: Sources, transport, and optical thickness. *Journal of Geophysical Research*, *99*(D11), 22897–22914. https://doi.org/10.1029/94jd01928

Tegen, I., & Lacis, A. A. (1996). Modeling of particle size distribution and its influence on the radiative properties of mineral dust aerosol. *Journal of Geophysical Research*, *101*, 19237–19244. https://doi.org/10.1029/95JD03610

Uno, I., Eguchi, K., Yumimoto, K., Takemura, T., Shimizu, A., Uematsu, M., et al. (2009). Asian dust transport one full circuit around the globe. *Nature Geoscience*, *20*, 557–560. https://doi.org/10.1038/ngeo583

Willmott, C. J., Rowe, C. M., & Philpot, W. D. (1985). Small-scale climate maps: A sensitivity analysis of some common assumptions associated with grid-point interpolation and contouring. *The American Cartographer*, *12*, 5–16. https://doi.org/10.1559/152304085783914686

Wu, L., Su, H., & Jiang, J. (2013). Regional simulation of aerosol impacts on precipitation during the East Asian summer monsoon. *Journal of Geophysical Research*, *118*, 6454–6467. https://doi.org/10.1002/jgrd.50527

Xian, P., Klotzbach, P. J., Dunion, J. P., Janiga, M. A., Reid, J. S., Colarco, P. R., & Kipling, Z. (2020). Revisiting the relationship between Atlantic dust and tropical cyclone activity using aerosol optical depth reanalyses: 2003–2018. *Atmospheric Chemistry and Physics*, *20*, 15357–15378. https://doi.org/10.5194/acp-20-15357-2020

Xie, X., Liu, X., Che, H., Xie, X., Li, X., Shi, Z., et al. (2018). Radiative feedbacks of dust in snow over eastern Asia in CAM4-BAM. *Atmospheric Chemistry and Physics*, *18*, 12683–12698. https://doi.org/10.5194/acp-18-12683-2018

Xie, X., Liu, X., Che, H., Xie, X., Wang, H., Li, J., et al. (2018). Modeling East Asian dust and its radiative feedbacks in CAM4-BAM. *Journal of Geophysical Research*, *123*, 1079–1096. https://doi.org/10.1002/2017JD027343

Xie, X., Wang, H., Liu, X., Li, J., Wang, Z., & Liu, Y. (2016). Distinct effects of anthropogenic aerosols on the East Asian summer monsoon between multi-decadal strong and weak monsoon stages. *Journal of Geophysical Research*, *121*, 7026–7040. https://doi.org/10.1002/2015jd024228

Yoshioka, M., Mahowald, N. M., Conley, A. J., Collins, W. D., Fillmore, D. W., Zender, C. S., & Coleman, D. B. (2007). Impact of desert dust radiative forcing on Sahel precipitation: Relative importance of dust compared to sea surface temperature variations, vegetation changes, and greenhouse gas warming. *Journal of Climate*, *20*, 1445–1467. https://doi.org/10.1175/jcli4056.1

Yue, X., Wang, H., Wang, Z., & Fan, K. (2009). Simulation of dust aerosol radiative feedback using the global transport model of dust: 1. Dust cycle and validation. *Journal of Geophysical Research*, *114*, D10202. https://doi.org/10.1029/2008jd010995

Zhang, X. Y., Arimoto, R., & An, Z. S. (1997). Dust emission from Chinese desert sources linked to variations in atmospheric circulation. *Journal of Geophysical Research*, *102*(DD23), 28041–28047. https://doi.org/10.1029/97JD02300

Zhang, X. Y., Gong, S. L., Zhao, T. L., Arimoto, R., Wang, Y. Q., & Zhou, Z. J. (2003). Sources of Asian dust and role of climate change versus desertification in Asian dust emission. *Geophysical Research Letters*, *30*, 012272. https://doi.org/10.1029/2003GL018206

Zhang, X. Y., Wang, Y. Q., Niu, T., Zhang, X. C., Gong, S. L., Zhang, Y. M., & Sun, J. Y. (2012). Atmospheric aerosol compositions in China: Spatial/temporal variability, chemical signature, regional haze distribution and comparisons with global aerosols. *Atmospheric Chemistry and Physics*, *12*, 779–799. https://doi.org/10.5194/acp-12-779-2012